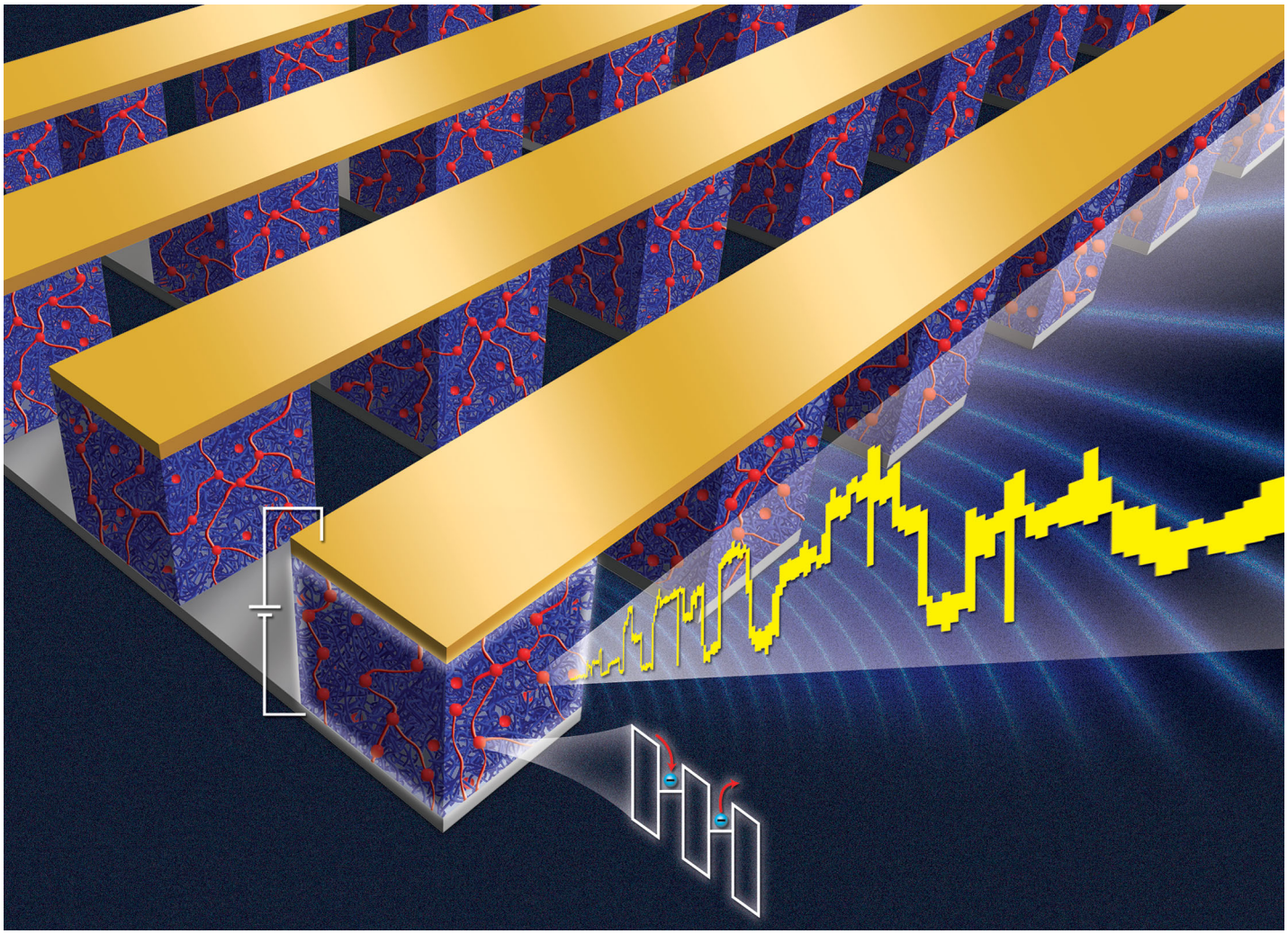

Showcasing research from Department of Physics and Astronomy, Seoul National University.

Electronic noise analyses on organic electronic devices

Telegraphic noise generated from electrically biased organic nanocomposite resistive memory devices. The telegraphic noise indicates a fluctuation of current pathways in the memory material.

As featured in:

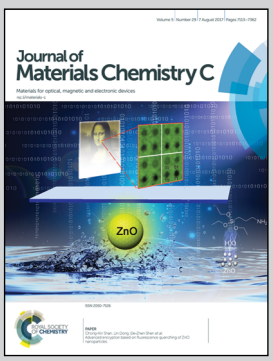

See Younggul Song and Takhee Lee,
J. Mater. Chem. C, 2017, **5**, 7123.

ROYAL SOCIETY OF CHEMISTRY

rsc.li/materials-c

Registered charity number: 207890

Journal of
Materials Chemistry C

REVIEW

View Article Online
View Journal | View Issue

Cite this: J. Mater. Chem. C, 2017, 5, 7123

Electronic noise analyses on organic electronic devices

Younggul Song and Takhee Lee *

Received 8th May 2017,
Accepted 26th June 2017

DOI: 10.1039/c7tc01997a

rsc.li/materials-c

In the past decade, considerable progress has been made in the field of organic electronic devices toward understanding charge transport processes and developing practical device applications. In addition, the electronic noise in organic electronic devices has been extensively studied along with the progress, providing a deep understanding of their electronic phenomena. This review article presents a summary of electronic noise analyses on various organic electronic devices to determine the usefulness of such analyses toward comprehending the operation of organic electronic devices. We expect that the noise analyses presented in this article will contribute to more meaningful insights for advancing organic electronic devices.

1. Introduction

Organic electronic devices (OEDs) embrace the advantages of low-cost, low-temperature, and solution-processed fabrication as electronics on large-area flexible platforms.[1–17] In addition, many researchers have been interested in the complex structures of the organic materials involved due to the irregular arrangement of their organic molecules, polymers, and trap-distributed structures.[18–34] Because noise spectra provide meaningful information on the structural or electronic disorder in organic materials, a number of researchers have conducted significant scientific studies on OEDs *via* noise analyses in the last decade.[35–78] Nevertheless, noise analysis methods for OEDs tend to be underestimated because of their seemingly inconclusive results. From this perspective, this review article addresses the motivation for studying electronic noises in OEDs and focuses on summarizing recent significant noise studies on various OEDs.

In this review article, three types of OEDs are discussed: organic thin film transistors (OTFTs), organic resistive memory devices, and molecular-scale electronic devices (Fig. 1). OTFTs are usually fabricated as top source–drain contact or bottom drain–source contact structures with a bottom gate electrode. The current/voltage fluctuations are measured at the drain electrode, while the constant voltage/current and constant gate

Department of Physics and Astronomy, and Institute of Applied Physics, Seoul National University, Seoul 08826, Korea. E-mail: tlee@snu.ac.kr; Fax: +82-2-884-3005; Tel: +82-2-880-4269

Younggul Song

Younggul Song is a PhD candidate in the Department of Physics and Astronomy, Seoul National University, Korea. He received his BS degree from Seoul National University, Korea, in 2010. He studies organic electronics, organic transistors and organic memory devices. Currently, his research focuses on the noise analyses on organic electronic devices.

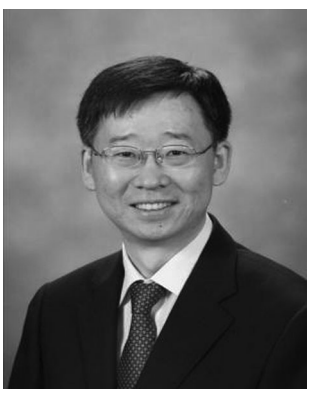

Takhee Lee

Takhee Lee is a Professor in the Department of Physics and Astronomy, Seoul National University, Korea. He received his BS and MS degrees from Seoul National University, Korea, and received his PhD from Purdue University, USA, in 2000. He was a postdoctoral researcher at Yale University, USA, until 2004. He was a Professor in the School of Materials Science and Engineering, Gwangju Institute of Science and Technology, Korea, from 2004 to 2011. His current research interests are molecular electronics, organic electronics, and physics of 2-dimensional films. He has written 10 book chapters, 13 review articles, and about 230 journal articles.

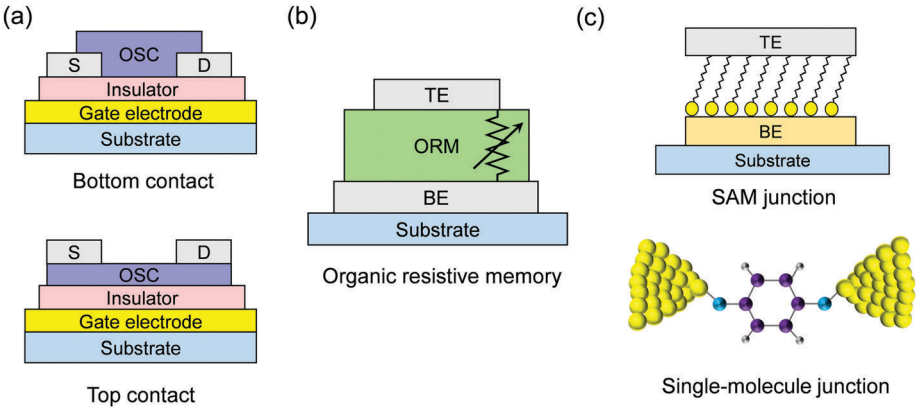

Fig. 1 Schematic diagrams of organic electronic devices. (a) Top drain–source contact (upper figure) and bottom drain–source contact (lower figure) organic TFT. (b) Organic resistive memory device. (c) Organic molecular devices with a SAM junction (upper figure) and a single-molecule junction (lower figure).

voltage are biased. Organic semiconductor materials are composed of organic molecules or polymers. They can be thermally evaporated or solution-processed on substrates. Noise analyses on OTFTs have provided insights into the fluctuation source (charge carrier number fluctuation or mobility fluctuation) and microscopic structure of the semiconductor molecules/polymer alignment. Organic resistive memory devices and molecular-scale electronic devices have usually been characterized in a two-terminal junction structure; hence, noise measurements can be performed by biasing one electrode while the other electrode is grounded. Organic resistive memory devices show bistable or multistable current–voltage (I–V) behavior. Their resistance can be changed by applying a set bias or reset bias. The switching mechanism and multistable behavior of organic resistive memory devices are still not clearly understood due to their highly disordered structures. Noise analyses on organic resistive memory devices can provide information relating their bistable behavior to the localized current pathways formed. Molecular-scale electronic devices make use of the physical properties of the extremely short channel lengths of organic materials, that is, the single-molecule length scale. There are two kinds of molecular-scale electronic devices: single-molecule junctions and self-assembled monolayer (SAM) junctions. The electrical characteristics of such devices depend on the structures, functional groups, and lengths of the organic molecules. Commonly, organic molecules used for molecular junctions contain a thiol group (such as hexanedithiol and benzenedithiol) to enable bonding with Au, which is a commonly used electrode. Noise analyses on molecular-scale electronic devices provide novel information about the traps inside the junction, the conformational and redox changes of the molecules, and the tunneling characteristics.

This review consists of four sections. In the Introduction section, we briefly presented the motivations and goals that drive noise analyses on OEDs (Section 1). Section 2 describes the background for conducting a noise analysis and the noise sources in OEDs. Section 3 addresses significant electronic noise analysis studies on organic thin film transistor devices (Section 3.1), organic memory devices (Section 3.2), and molecular-scale electronic devices (Section 3.3). Section 4 provides a summary and desired prospects for electronic noise analysis on OEDs.

2. Fundamental description of the noise analysis of an electronic device

The noise in electronic devices is usually measured by biasing the current or voltage of the device. If a device is biased using the voltage, one can measure the current noise and *vice versa*. The fluctuation in the current and voltage response in the time domain can be sampled using a specific time interval. Let us denote the fluctuation in the voltage, current or resistance recorded with time as $X(t)$, which by itself can provide useful information if it shows random telegraph noise in which a number of stable current levels exist. However, in most cases, $X(t)$ is the result of the superposition of various noise signals, such as flicker noise, thermal noise, shot noise, and Lorentzian noise. Therefore, it is more useful to investigate the noise spectra by decomposing each frequency component from $X(t)$. With this requirement, estimating the power spectral density is the most preferable way to analyze the noise data. To estimate the power spectral density, one needs to calculate the autocorrelation function ($A(\tau)$) of $X(t)$.[79]

$$A(\tau) = \langle X(t+\tau)X(t)\rangle \quad (1)$$

Then, the Fourier transform of the autocorrelation function when multiplied by two results in the power spectral density ($S_X(f)$).

$$S_X(f) = 2\int_{-\infty}^{\infty} \mathrm{d}\tau \mathrm{e}^{i\omega\tau} A(\tau) \quad (2)$$

This relation between the power spectral density and time series is mathematically well defined and is called the Wiener–Khintchine theorem. The autocorrelation function determines the correlation between two data points with an interval of τ, revealing the characteristics of the noise process. For example, for white noise, $A(\tau) = \delta(\tau)$, showing the constant

frequency dependence of $S_X(f)$. The physical meaning of the power spectral density is the frequency component of the noise power average per unit frequency band. The noise power average, which is the mean squared signal of the variance of the fluctuations, can be expressed as the integral of $S_X(f)$ over all positive frequencies.

$$\langle (\delta X)^2 \rangle = \int_0^\infty \mathrm{d}f S_X(f) \quad (3)$$

Noise spectra in electronic devices are classified into several types according to their noise sources or frequency dependence. There are four important types of noise in this review: thermal noise, shot noise, random telegraph noise, and $1/f$ noise. Table 1 summarizes the noise types reported in OEDs.

2.1. Thermal noise

The thermal motion of charge carriers can cause random fluctuations in the current, which is called thermal noise (Johnson–Nyquist noise).[79] The thermal noise is determined by only the dissipative nature of the conductor (resistance (R) and temperature (T)), which can be derived from the fluctuation–dissipation theorem (this is why the thermal noise is called equilibrium noise). The expression for the thermal noise is frequency independent in the quasi-classical regime ($hf \ll k_\mathrm{B}T$):[79]

$$S_V = 4k_\mathrm{B}TR;\ S_I = 4k_\mathrm{B}T/R \quad (4)$$

where S_V is the voltage noise power spectral density, S_I is the current noise power spectral density and k_B is the Boltzmann constant. The thermal noise shows white noise (constant power spectral density) under usual experimental conditions (for example, the quasi-classical regime holds up to 10^{11} Hz at 4 K). Because the thermal noise is not affected by the microscopic structure of the organic material and is affected by only R and T, the thermal noise itself may not be considered to be an interesting topic in organic electronics. However, one should carefully consider the thermal noise during noise measurements because the thermal noise can hinder the noise of interest within a certain range of the frequency band.

2.2. Shot noise

In the classical sense, shot noise is caused by the discrete nature of charge carriers and the randomness of the arrival of independent charge carriers into channels in a nonequilibrium system, such as an electrically biased system. A current flow is required to observe the shot noise. In this case, the randomness stems from fluctuations in the reservoirs before the channel and shot noise can be modeled by a Poisson process.[80,81] Considering quantum mechanics and mesoscopic systems, the scattering properties (transmission and reflection) inside the channel and Fermi–Dirac statistics should be accounted for the random arrival of charge carriers. Shot noise is found in various electronic systems, such as vacuum tubes[82] and semiconductor diodes,[83] and mesoscopic systems, such as quantum contact points,[84,85] chaotic cavities,[86] and metallic diffusive wires.[87,88] Shot noise can be expressed as[80]

$$S_I = 2qF|\bar{I}| = \frac{2qF|V|}{R} \quad (5)$$

where q is the electronic charge, R is the resistance, and F is called the Fano factor, which is introduced as an adjustment factor to indicate the variance in the Poisson value. Shot noise shows a white spectrum up to the frequency limit of $f_\mathrm{p} = 1/\tau_\mathrm{p}$, where τ_p is the duration of each pulse. The F value becomes 1 in the classical limit with a very small transmission rate, a high temperature and the absence of correlation between the charges. The F value is determined by the mesoscopic properties of the channels and the interactions between the charge carriers. According to the transmission probability, the Fano factor can be between 0 (an open channel) and 1 (a perfectly transmitting channel), and the noise can be called sub-Poissonian shot noise. The Fano factor can be greater than 1 if the Coulomb repulsion and phonon interactions cannot be ignored. For example, shot noise has been reported in organic light-emitting diodes at room temperature.[89] Noticeably, shot noise in single-molecule junctions has been studied very carefully recently because shot noise can provide information about the mesoscopic properties as modulated by the molecules inside the junction (see Section 3.3.2).

Table 1 Electronic noise types which are observed in organic electronic devices

Noise type	Noise source	Device	Power spectral density
Thermal noise	– Thermally induced motions of charge carriers	– Any resistor	$S_I = \frac{4k_\mathrm{B}T}{R}$
Shot noise	– Discrete nature of charge carriers – Random arrival of charge carriers at the channel	– Single-molecule junctions	$S_I = 2qF\|I\|$
Random telegraph noise	– Trap/detrap of charge carriers at the trap center – Conformational change of molecules	– Metal-oxide polymer resistive memory – Organic nanocomposite resistive memory – SAM junctions – Single-molecule junctions	$S_I \propto \frac{1}{1+(2\pi f\tau_0)^2}$
$1/f$ noise	– Explicit source is unknown	– Organic thin film transistors – Metal-oxide polymer resistive memory – Organic nanocomposite resistive memory – SAM junctions – Single-molecule junctions	$S_I \propto \frac{1}{f}$

2.3. Random telegraph noise

Random telegraph noise (RTN) indicates an electronic noise in which discrete random transitions appear between two or more voltage/current levels. RTN has been observed in various electronic systems, such as metal-oxide–semiconductor field effect transistors (MOSFETs),[90–92] resistive memory devices,[93–95] point contacts,[96] and nanogap junctions.[97,98] Generally, RTN is known to be generated by the contribution of thermally activated transitions or tunnel transitions between energy wells.[99] In the case of the two-level RTN observed in MOSFETs, it is well known that the charge trapping/detrapping at a single trap inside the oxide layer is responsible for the RTN.[79,100,101] In oxide-based resistive memory devices, RTN has been reported for various resistance states and has usually been attributed to the traps distributed in the oxide memory material.[102–104] With the exponential decay of $A(\tau)$ ($\sim\exp(-\tau/\tau_0)$, where τ_0 is the relaxation time of the random telegraph noise), two-level RTN is known to exhibit a Lorentzian power spectral density[79]

$$S_I \propto \frac{1}{1+(2\pi f\tau_0)^2} \tag{6}$$

However, the power spectral density cannot provide all the useful information regarding RTN because alterations in the conductance states and the amplitude levels between the states cannot be clearly deduced from the power spectra. Therefore, when analyzing RTN, time domain measurements and their direct statistical analyses are important for understanding the physical nature of the system. For example, the mean spent time (τ_2 and τ_1) in each state of two-level RTN is usually found to have an exponential relation to the inverse of temperature ($1/T$):[79,90,105]

$$\tau_1 \propto \exp\left(\frac{E_1}{k_B T}\right), \tau_2 \propto \exp\left(\frac{E_2}{k_B T}\right) \tag{7}$$

where E_1 and E_2 are the activation energies of each state. In organic electronic devices, RTN has been observed in organic resistive memory devices (Section 3.2), SAM junctions (Section 3.3.1), and single-molecule junctions (Section 3.3.2) due to contributions from the traps or conformation changes in the molecules.

2.4. 1/*f* noise

Specified by its name, any electronic noise that exhibits a power spectrum density with a $1/f^{\gamma}$ frequency dependence ($0.9 < \gamma < 1.1$) is called $1/f$ noise. This type of noise can be observed in most semiconductor systems, such as MOSFETs,[106–108] bipolar junction transistors (BJTs),[109] thin film transistors,[110,111] light emitting diodes,[112,113] solar cells,[114] magnetic random access memory (MRAM) devices,[115] flash memory devices,[116] and resistive random access memory (RRAM) devices.[95,117–119] Because $1/f$ noise appears ubiquitously in electronic systems from the bulk size to molecular size and from crystals to disordered systems, a well-defined process or mechanism explaining all the $1/f$ noises in various systems does not exist. However, there are a number of insightful explanations that are limited to specific ranges of systems. In the field of semiconductor physics, a tremendous number of studies have been conducted since the 1950s regarding the analysis of $1/f$ noise in semiconductors.[79,120–126] Here, we introduce representative explanations that will be helpful for understanding this review. In the 1950s, McWhorter suggested that $1/f$ noise is caused by charge carrier number fluctuations at the interface between the semiconductor and oxide.[121,126] In oxides, the traps are distributed uniformly, and charge carriers in the semiconductor can be trapped and detrapped at the oxide traps, causing number fluctuations in the conductive charge carriers. These fluctuations are called generation–recombination (GR) noise and exhibit a Lorentzian spectrum for a single trap. Because there are a number of traps inside the oxide, the resultant noise is the superposition of the GR noises with different characteristic times for each trap. If the traps are distributed uniformly in the oxide and electrons can be trapped due to tunneling, the distribution of the characteristic times is proportional to $1/\tau$. For the distribution in the range of τ_1 and τ_2, $1/f$ noise can occur in the range of $\tau_1 < \tau < \tau_2$ due to the superposition of the GR noises. McWhorter's description provides a very useful framework for understanding $1/f$ noise, so the description has been employed for describing the noise in various FET systems.

In the 1960s, Hooge proposed a universal empirical relation from a number of noise measurements in metals and semiconductors, which is called Hooge's empirical relation.[121,122,127,128]

$$\frac{S_R}{R^2} = \frac{S_I}{I^2} = \frac{S_V}{V^2} = \frac{\alpha}{f N_c} \tag{8}$$

where α is called the Hooge parameter and N_c is the total number of free charge carriers inside the material. The relation describes the bulk noise inside a specimen, as indicated by N_c. Initially, α was found to be approximately 2×10^{-3} for ohmic homogeneous samples, and it was considered to be a universal constant. However, in later studies, α was found to be dependent on the temperature, magnetic field, crystallinity, and material type. Therefore, Hooge's relation is not a universal relation, although the relation can be considered as a useful standard for noise experiments. In homogeneous and ohmic samples, the measured α value does not deviate by more than two orders of magnitude from 2×10^{-3}. Strongly disordered and inhomogeneous samples can have α values many orders greater than 2×10^{-3}, as the effective number of free charge carriers may be much smaller than N_c. In organic semiconductor devices, all α values have been measured to be greater than 2×10^{-3}, depending on the material type and device structure. Based on Hooge's empirical relation, the bulk mobility fluctuation induced by charge scattering has been considered to result in $1/f$ noise.[129]

In the 1990s, researchers tried to explain $1/f$ noise in MOSFET devices as the contribution of both number fluctuations and mobility fluctuations.[92,130] The fluctuations in the oxide trap occupancy can affect the scattering rates and cross sections of the charge carriers in a semiconductor and are referred to as correlated fluctuations between the carrier number and surface mobility. One of the most widely used noise relations

for correlated fluctuations was proposed by Ghibaudo *et al.* and is expressed as[130]

$$\frac{S_I}{I^2} = \left(1 + \alpha_{sc}\mu_{eff}C_{ox}\frac{I_{SD}}{g_m}\right)^2\frac{{g_m}^2}{{I_d}^2}S_{fb} \quad (9)$$

where α_{sc} is the scattering coefficient, μ_{eff} is the effective mobility, I_{SD} is the source–drain current, C_{ox} is the gate oxide capacitance, g_m is the gate transconductance and S_{fb} is the flat band voltage spectral density. Note that this relation cannot explain the origin of 1/*f* noise; however, one can inspect the dependence of the noise on I_D and g_m and then check the degree of the noise correlations with the gate oxide charge trapping fluctuations.

In organic electronic devices, 1/*f* noises have been found in almost all the devices, and they depend on the gate voltage, luminescence, voltage bias regime, resistance, and microscopic structure. Although 1/*f* noises in disordered organic materials are hard to explain, analyzing their dependence on various factors has provided meaningful insights into the charge transport mechanisms and microscopic structures of organic materials.

3. Noise analyses on OEDs

3.1. Noise analyses on organic thin film transistor (OTFT) devices

Because the device structures of OTFTs are similar to those of MOSFETs and inorganic thin film transistors, the noise analysis methods developed with MOSFETs and inorganic transistors have been introduced to study the electronic noise in OTFTs, for example, regarding Hooge's empirical relation, trapping–detrapping fluctuations at the interface, and charge number–mobility correlated fluctuations. Meanwhile, the effects of the own characteristics of OTFTs such as disordered microstructure, distributed traps, and interfacial treatment on the electronic noise have also been studied. Here, we present several examples.

3.1.1. Mobility fluctuations *vs.* number fluctuations. From Hooge's empirical relation, $S_I/I^2 \propto N^{-1} = q\mu\rho/V$, where μ is the mobility of free charge carriers, ρ is the resistivity, and V is the volume of the resistor. One way to check whether the subject system follows the empirical relation is to measure the relative noise by varying the number of free charge carriers, N. Vandamme *et al.* studied the noise characteristics of poly(thienylene vinylene) (PTV) and pentacene transistors by varying the channel lengths, gate biasing, and illumination and indicated an inversely proportional relation between the relative noise and N.[35] The PTV samples showed 1/*f* noise, and $S_I \propto I^2$ in the ohmic range of the applied source–drain voltage, V_{ds} (Fig. 2a). The extracted Hooge parameters were in the 0.01–0.08 range. In the ohmic range, they investigated the relation between S_I/I^2 and the source-gate voltage, V_{gs} (Fig. 2b). From a simple capacitor consideration ($Nq = C_{di}(V_{gs} - V_{th} - V_{ds}/2)$,[38,131] where C_{di} is the capacitance of the dielectric layer, V_{th} is the threshold voltage, and V_{ds} is the source–drain voltage), $S_I/I^2 \propto {V_{gs}}^{-1}$ can be observed with small V_{th} and V_{ds} values relative to V_{gs}. They measured this inversely proportional relation in the −9 V to −22 V V_{gs} range. In addition, N can be controlled by modulating the channel volume with different channel lengths, L. They measured PTV samples with different channel lengths (5, 10, 20, and 40 μm) and found $S_I/I^2 \propto L^{-1}$, which is in agreement with the empirical relation for ohmic samples (Fig. 2c). Pentacene is known for its photoresponse property.[36,37] While extra free charge carriers are generated in pentacene samples under illumination, the sample resistance decreases ($R \propto N^{-1}$). By varying the illumination intensity, Vandamme *et al.* found that $S_I/I^2 \propto R$, which supports the empirical relation (Fig. 2d). An inversely proportional relation to V_{gs} has also been reported in other studies on pentacene transistors[38] and UV-treated pentacene transistors.[40] Jia *et al.* observed similar illumination effects on their UV-treated pentacene transistors, suggesting that mobility fluctuations were dominant in their samples.[40] Marinov *et al.* performed mobility and noise inspections on polymer thin film transistors (3-hexadecylthiophene).[41,42] From the power law relation between noise and mobility and the proportionality between the noise and DC power ($I_d \times V_{ds}$), they concluded that the low frequency noise originated from mobility fluctuations in the polymer layer. The hopping process of the charge carriers in the polymer layer was suggested to be the origin of the mobility fluctuations.

Regarding number fluctuations, Martin *et al.* suggested that carrier trapping and detrapping at the intergrain traps of organic semiconductors provide the sources of 1/*f* noise in OTFTs, and the noise level could be further lowered by controlling the degree of ordering in the molecules within the grains.[43] Ke *et al.* suggested that number fluctuations due to grain boundaries dominate at low drain currents and the other number fluctuations due to the interfacial oxide traps dominate at large drain currents.[44] Moreover, Kang *et al.* investigated the noise properties of thermally evaporated pentacene OTFTs with various grain sizes and thicknesses.[45] All the devices showed $1/f^{\gamma}$ noise; however, different γ values were observed depending on the thickness, grain size, and gate bias (Fig. 3a). In the saturation regime, all the devices showed γ values greater than 1 and close to 1.4–1.5. Increased γ values in the saturation regime were also observed in the follow-up noise study on poly(2,5-bis(3-alkythiophen-2-yl)thieno[3,2-*b*]thiophene) (pBTTT) TFTs.[46] The thickness did not affect the noise characteristics of the OTFTs because it is known that accumulated charges reside in the first 1–2 monolayers.[47,48] The increased γ values in the saturation regime and the linear regime were attributed to the involvement of deep traps at the grain boundaries. In the saturation regime, the Fermi level around the drain electrode is located near the mid gap of organic semiconductors; hence, deep traps at the mid gap are involved in the number fluctuations, with slower processes than those of shallow traps. Then, the low frequency component increases, explaining the higher γ values in the saturation regime. If these number fluctuations can be considered as the superposition of Lorentzian noise from the interfacial traps, the distribution of traps involved in the number fluctuations can be changed with the saturation regime, resulting in a change in the γ values.[121] Fig. 3b shows a $S_I/{I_d}^2$–I_d plot fitted using eqn (9), which indicates that the noise in OTFTs is related to the trapping noise model with correlated mobility fluctuations.[130] Kang *et al.* suggested that

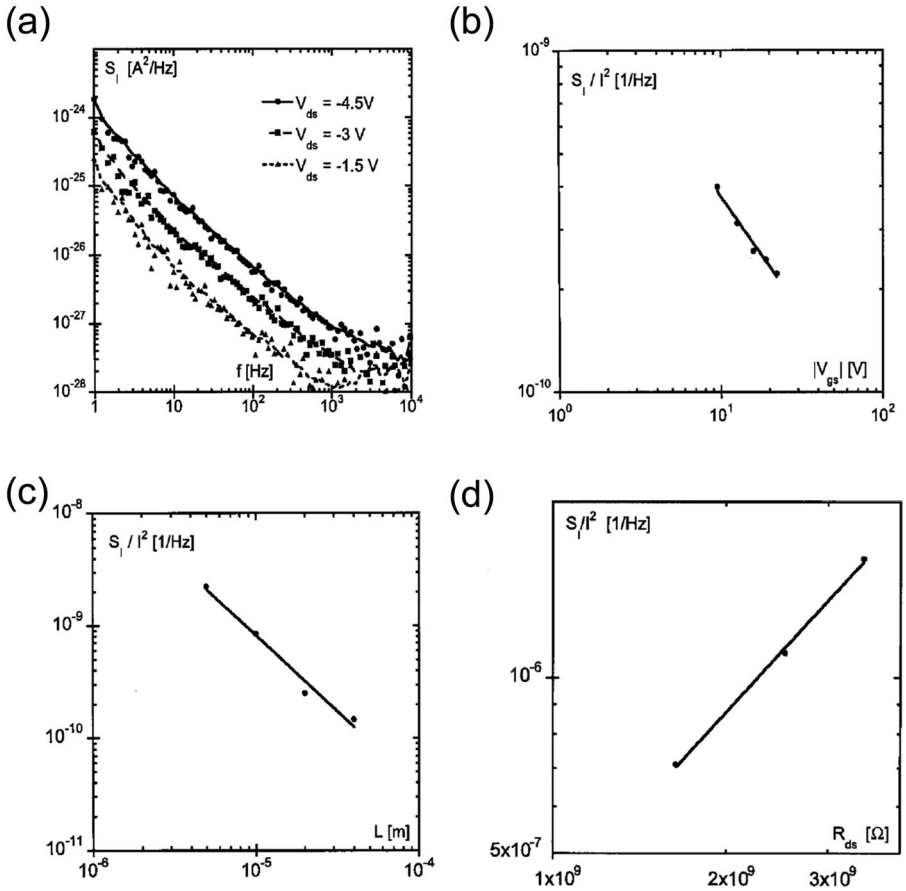

Fig. 2 Noise characteristics of OTFTs and inversely proportional relationship between charge carrier numbers N and relative noise S_I/I^2. (a) Current noise spectra S_I in a poly-thienylene vinylene (PTV) sample. The spectra show $1/f$ and background noise. (b) The relative noise S_I/I^2 taken at f = 1 Hz dependence on the gate voltage V_{gs}. (c) Geometry dependence of the relative noise on a PTV sample (taken at 1 Hz with V_{ds} = −3 V and V_{gs} = −15.9 V). (d) Illumination effects on the relative noise on a pentacene sample. Reproduced with permission from ref. 35, Copyright 2001, AIP Publishing LLC.

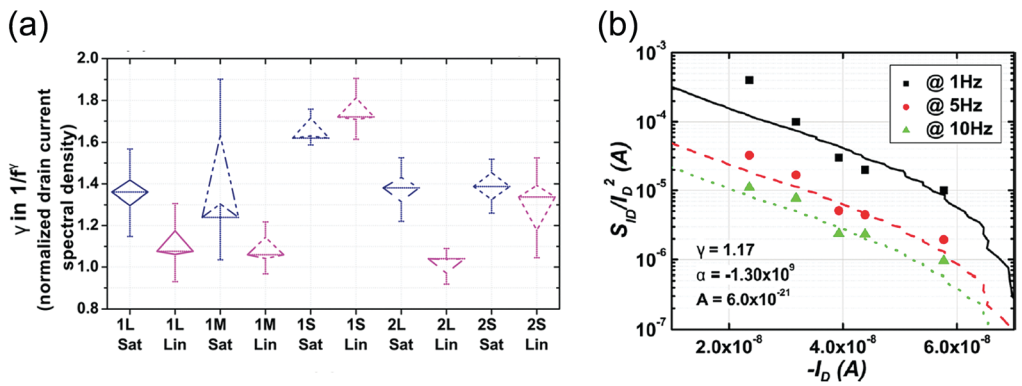

Fig. 3 Noise-generation phenomena in OTFTs as carrier trapping by traps. (a) Distribution of exponent values of $1/f^{\gamma}$ for the pentacene OTFT with different grain sizes (L: 4 μm^2, M: 3 μm^2, S: 1 μm^2 of grain sizes), thicknesses (1: 14 nm, 2: 26 nm) and operating regimes (Sat: saturation, Lin: linear). Diamond boxes in the graph define the boundary of standard errors, and whiskers in the graph show the boundaries of standard deviations. (b) Application of the unified noise model to the normalized drain current spectral density of the sample 1L in the linear region. Reproduced with permission from ref. 44, Copyright 2011, AIP Publishing LLC.

carrier density fluctuations and mobility fluctuations due to Coulomb scattering at traps can explain the low frequency noise of OTFTs. Similarly, evidence for the correlated mobility fluctuations in OTFTs was obtained by fitting the quadratic relation between the gate voltage noise (S_{VG}) and I_d/g_m in eqn (9).[49,50]

3.1.2. Effect of the microstructure in OTFTs. OTFTs with bottom source–drain contact (BC) structures have usually

exhibited inferior device performance compared to top source–drain contact (TC) structures because of the poor morphology of organic films on metal electrodes.[51,52] The carrier mobility doubled in TC structures due to better injection of the charge carriers. Necliudov *et al.* compared $1/f$ noises from TC and BC pentacene OTFTs.[53] They reported that the S_V showed clear $1/f$ noise in TC and BC devices and showed a 10 times higher level for the BC device than the TC device. The extracted Hooge parameters were three orders of magnitude larger for the BC devices than those of the TC devices (α_{BC} = 5–20 and α_{TC} = 0.045). They provided key evidence that the interface and contact properties can meaningfully affect the noise characteristics.

The mobility of organic transistors is known to be dependent on the thickness and morphology of the thin active organic semiconductor layers. For vacuum-deposited organic semiconductors, such as pentacene and copper-phthalocyanine, the field-effect mobility depends on the number of stacked semiconducting layers, showing scaling behavior between the mobility and thickness up to 10 layers.[47,132] This scaling behavior suggested the percolation conducting behavior of OTFTs caused by the disordered structures of the grain boundaries (Fig. 4a). Grain boundaries form intrinsic energy barriers and trapping centers that can block charge transport due to high barrier heights and charge accumulation.[54,55] Conrad *et al.* measured the current noise of pentacene films with different film thicknesses and the noise-mobility scaling behavior, which indicated percolative effects in pentacene transistors.[38] They treated the pentacene transistors as a mixture of conducting and insulating components that followed a percolation model. Note that percolative conducting networks exhibited noise scaling behavior: $S_I/I^2 \propto \rho^{\omega}$.[79] Assuming a fixed number density, this scaling relation becomes $S_I/I^2 \propto \mu^{-\omega}$. Treating the device as a simple parallel plate capacitor, the assumption of a fixed number density is reasonable. With various pentacene thicknesses (7 nm to 40 nm), the Hooge parameter *versus* the film thickness and the mobility *versus* the film thickness were measured, respectively (Fig. 4b and c). After combining the relations, the Hooge parameter and mobility followed the scaling behavior of $\alpha_H \propto \mu^{-\omega}$ (ω = 2.9 ± 0.4) under a 20 nm film thickness. Conrad *et al.* concluded that this scaling behavior was attributed to current crowding in the pentacene films as inhomogeneous systems in which the charge carrier transport was disrupted by the grain boundaries.[38]

In the case of BC structures, the microstructure or organic thin film near the source/drain electrodes can be controlled using surface chemical treatments on the electrodes.[133] Specifically, a solution-processed fluorinated 5,11-bis(triethylsilylethynyl)anthradithiophene (diF-TESADT) transistor with pentafluorobenzenethiol (PFBT)-treated bottom source/drain electrodes showed larger grain sizes near the electrodes and better electronic characteristics.[56–58] Jurchescu *et al.* observed the correlations between microstructure changes and $1/f$ noise in diF-TESADT TFTs (Fig. 5).[39] They prepared three types of samples with bottom-contacted Au electrodes. No contact treatment was applied to type 1 devices. For type 2 devices, the source/drain bottom electrodes were treated with PFBT. For type 3 devices, the bottom electrodes

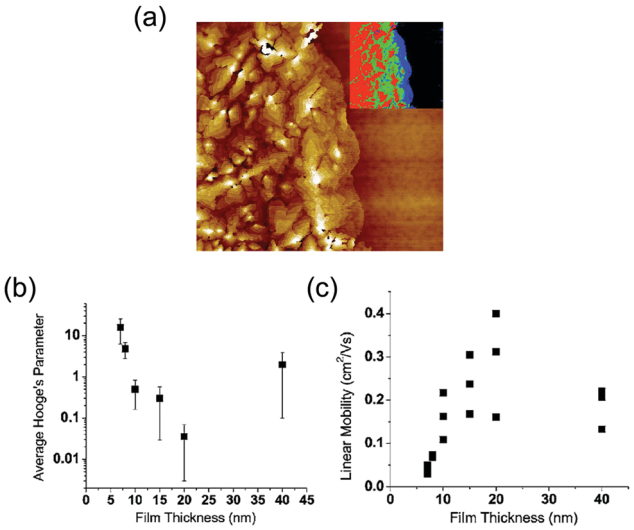

Fig. 4 Percolative effects indicated by the spectral noise. (a) (20 μm)^2 atomic force microscopy image of the channel edge of a 7 nm-thick pentacene film. Inset: (blue) the first pentacene layer, (green) the second and third pentacene layers, and (red) more than three layers. (b) Average Hooge's parameter and mobility as functions of the pentacene film thickness. Combining the relations (b) and (c) with film thicknesses below 20 nm, one can obtain the relation $\alpha_H \propto 1/\mu^{\omega}$, where ω = 2.9 ± 0.4. Reproduced with permission from ref. 38, Copyright 2007, AIP Publishing LLC.

were treated with PFBT, and the oxide insulator was treated with hexamethyldisilazane (HMDS). Then, dif-TESADT films were spin cast onto the electrodes. For the type 2 devices, highly crystalline grains were formed on and near the bottom electrodes (Fig. 5a and b). For the type 1 devices, the highly crystalline grains showed no significant growth at the contact edges (Fig. 5c). For the type 3 devices, the highly crystalline grains were extended throughout the entire channel due to the gate oxide treatment with HMDS (Fig. 5d). The field effect mobilities and relative noise (S_I/I^2) were plotted along the channel lengths (Fig. 5e). The current noise in all the device types exhibited $1/f^{\gamma}$-type noise, with $0.85 < \gamma < 1$. The mobilities showed exponential decay with increasing channel lengths, which might have indicated a percolation effect due to the presence of inhomogeneous conductors.[59] At short channel lengths smaller than 25 μm, the type 3 devices showed the highest relative noise, and the type 1 devices showed the lowest relative noise, which implies that better crystalline grains generate less electronic noise. The sudden changes in the mobility decay rate and the rapid decrease in the relative noise levels corresponded well to the morphological changes in Fig. 5a–d. When less crystalline grains formed at the middle of the channel, higher noise was generated due to the larger number of grain boundaries. It is notable that the noise measurements were sensitive to the formation of poorly ordered regions.

Defects are distributed in organic semiconductors where traps are formed due to chemical impurities, grain boundaries, and sliding between molecules.[134] The charge carrier transport in organic semiconductors is known to occur due to hopping between localized electronic states. While Conrad *et al.* showed that percolation behavior is caused by grain boundary formation,[38]

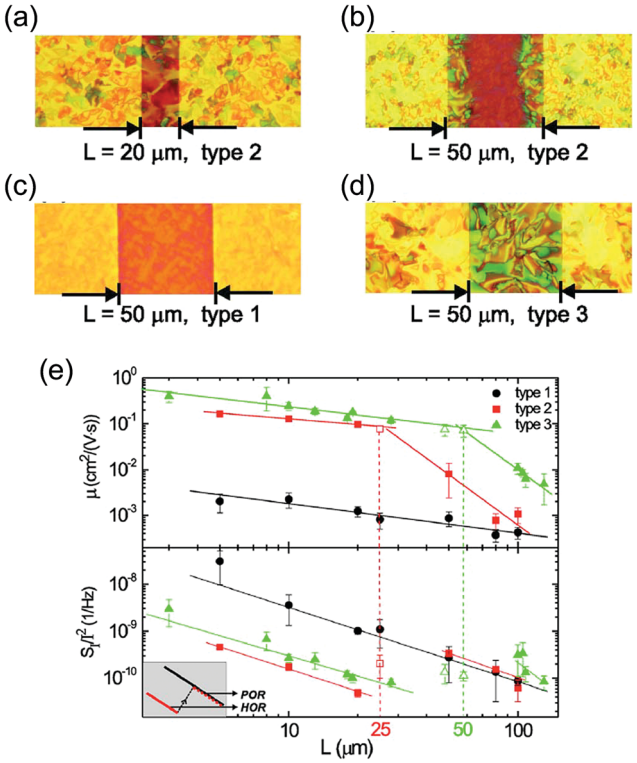

Fig. 5 Microstructure effects of OTFTs on the relative noise amplitudes. (a–d) Optical micrographs of the three types of contact-treated organic transistors. No contact treatment was applied to type 1 devices. The contacts were treated with pentafluorobenzenethiol for type 2 and type 3. An extra step of HMDS treatment on the gate dielectric was used for type 3. (e) Saturation mobility μ *vs.* channel length L for diF-TESADT TFTs (upper graph). Normalized spectral density (S_I/I^2) at f = 100 Hz for the same devices. Reproduced with permission from ref. 39, Copyright 2008, AIP Publishing LLC.

Carbone *et al.* showed that voltage-controlled trap filling inside pentacene can also cause percolation effects.[60] Sandwich structures (Au/pentacene/Al) were used in their study to exclude the interfacial trap effect. In this diode-type structure, organic semiconductors are known to exhibit space-charge-limited current (SCLC) behavior related to the trap-filling effect.[61–63] In the sandwiched pentacene samples, three transport regimes were observed in the I–V characteristics: the ohmic regime ($I \sim V$ at 0.3–0.8 V), trap-filling regime ($I \sim V^{5.1}$ at 0.8–2 V), and SCLC regime ($I \sim V^2$ at >2 V). The noise spectra exhibited $1/f$-type noise, and they observed peculiar changes in the relative noise amplitude (Fig. 6). In the ohmic regime, the relative noise amplitudes remained the same as the voltage changed. In the trap-filling regime, the relative noise increased with voltage. Then, the amplitude decreased in the SCLC regime as approximately $1/V$, according to a noise suppression mechanism. Then, the noise peak in which the relative amplitude became maximum could be observed within the trap-filling regime. In the ohmic regime, the conductive component consisted of thermally excited charge carriers. In the SCLC regime, the deep traps were almost completely filled so that the charge transport was dominated by space charge-controlled injected holes. In the trap-filling regime, the system could be seen as a continuum percolative medium in which the conductive phase (ohmic regime) and the insulating phase (SCLC region) competed with each other. Then, the noise peak could be understood as the critical behavior. In the trap-filling region, percolative scaling between the relative noise and conductive volume fraction (ϕ) is expressed as

$$\frac{S_I}{I^2} \propto (\phi - \phi_c)^{-k} \propto (n - n_t)^{-k} \quad (10)$$

where ϕ_c is the critical conductive volume fraction, k is a critical exponent, n is the free carrier density, and n_t is the trapped carrier density. Upon increasing the voltage bias, charge carriers become trapped in deep traps within pentacene with increasing n_t. Then, at the point where $n = n_t$, the noise peak could be observed. Carbone *et al.* further developed a noise model, which provides a quantitative interpretation between the relative current noise and applied voltage.[64] The noise model includes the noise generated in the ohmic, trap-filling, and SCLC regimes ($S_I/I^2 = S_{ohm}/I_{ohm}^2 + S_{TF}/I_{TF}^2 + S_{SCLC}/I_{SCLC}^2$).

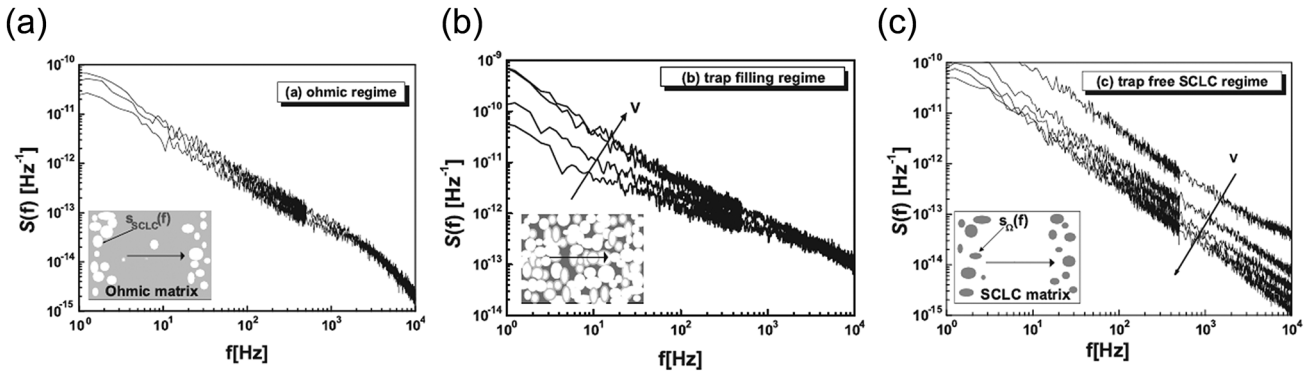

Fig. 6 Noise spectra for the Au/Tc/Al sample. (a) Ohmic regime: relative noise does not vary with V in the ohmic regime (0.3–0.8 V). (b) Trap-filling regime: relative noise sharply increases with V during the trap-filling transition (0.8–2 V). (c) Space-charge-limited current regime: relative noise decreases approximately as $1/V$ (>2 V). The two-phase medium is shown in the insets. The horizontal arrows represent the current direction. The white areas represent filled traps, *i.e.*, insulating sites characterized by $s_{SCLC}(f)$ noise. The dark areas represent empty traps, *i.e.*, conductive sites characterized by $s_\Omega(f)$ noise. Reproduced with permission from ref. 60, Copyright 2005, American Physical Society.

3.1.3. Statistics of 1/*f* noise in OTFTs. According to Marinov and Deen's work on the collection of low-frequency noises in OTFTs, almost all the OTFTs exhibited $1/f^{\gamma}$ noise with $\gamma = 1.042 \pm 0.08$ (Fig. 7a).[65] Marinov and Deen rearranged these data into a function of the relative noise amplitude and device channel area, and compared them to various inorganic TFTs[66] (MOSFETs, BJTs, nanowires, and carbon nanotubes) (Fig. 7b). The reciprocal relationship between the relative noise amplitude and active area of a device ($f \cdot S_I/I^2 \propto (WL)^{-1}$) is a well-established scaling rule because it can be described using Hooge's empirical relation, the interfacial trapping model, and the variable-range hopping fluctuation model.[65] It is notable that the relative noise amplitudes of OTFTs are about three orders of magnitude higher than those of inorganic transistors. Therefore, the LFN generation after downscaling OTFTs into microsized channel dimensions should be carefully considered. Another observation in Fig. 7b is that the deviations from the scaling trends for the OTFTs and inorganic transistor devices were on the same order of magnitude ($\sigma \sim 9$ dB$_{10}$). The deviations in OTFTs may have originated from the diverse fabrication processes used. And the same order of deviations between inorganic and organic devices meant the diversities in the OTFT fabrication and the inorganic devices were similar in the magnitude order. Marinov and Deen noted that a single noise model could not fully explain the behavior of all OTFTs due to this diversity.

3.2. Noise analyses on organic memory devices

Organic resistive memory devices have multiple resistive states when the applied bias is modulated. There are several material and structural types of organic resistive memory devices, such as single-layers, bilayers, embedded structures, and nanocomposite layers.[135] Various types of organic resistive memory devices have been fabricated, electrically characterized, and utilized. However, the switching mechanisms of organic resistive memory devices are still debated because of their highly disordered structures and variability. In this regard, noise analyses can provide an influential way to understand the resistive switching in a statistical sense. The electronic noise from various conductive states (low or high resistance states and the resistance state near switching occurs) can be analyzed, indicating each noise source at the resistance state. Profound noise analyses have been performed on single-layer type organic memory devices with metal oxide interfaces and organic nanocomposite type memory devices regarding the localized current pathway formation and percolation behavior.

3.2.1. Metal-oxide polymer resistive memory devices. Rocha *et al.* measured the current noise characteristics of metal-oxide polymer memory devices and concluded the formation of filamentary conduction pathways in their memory devices.[67] The interface between a sputtered Al_2O_3 layer and spirofluorene polymer layer was crucial for the resistive switching behavior. In their memory devices, the *I–V* characteristics showed unipolar bistable behavior with negative differential resistance (NDR) (Fig. 8a). In addition, $1/f^{\gamma}$ noises with $\gamma = 1$ and 1.5 were measured at a low voltage (0.5 V, on state) and near the NDR (5 V) (Fig. 8b), respectively. At 0.5 V, the relative amplitude of the $1/f$ noise ($C_{1/f} = fS_I/I^2$) was higher (1.8×10^{-6} cm^2) than the $C_{1/f} \approx 10^{-18}$ cm^2 measured from the $1/f$ noise in tunnel junctions.[68] The high amplitude of the $1/f$ noise was expected in the case of low numbers of free charge carriers or the constriction of charge carrier flow. Fitting the *I–V* characteristics to the Mott–Gurney law, a 10^2 smaller effective area compared to the real device area was calculated in their discussion, also indicating the presence of localized conduction in the resistive memory devices. The exponent $\gamma = 1.5$ at 5 V (near the NDR) suggested that a different mechanism dominated over $1/f$ noise. The value of 1.5 was attributed to the diffusion of defects related to the conducting spots in the Al_2O_3 layer. After quasistatic capacitance–voltage and electroluminescence experiments on the same memory system, Bory *et al.* concluded that the bistable behavior originated from conducting filaments and charge trapping at the interface of the Al_2O_3 and polymer layers. To explain these results, they introduced a quasiparticle that consisted of a trapped electron at the organic semiconductor interface and a trapped hole (called ionized defects) at the metal oxide interface.[69] The domains with ionized defects had a low work function; hence, these regions could enable the injection of electrons (current filaments) (Fig. 8c).

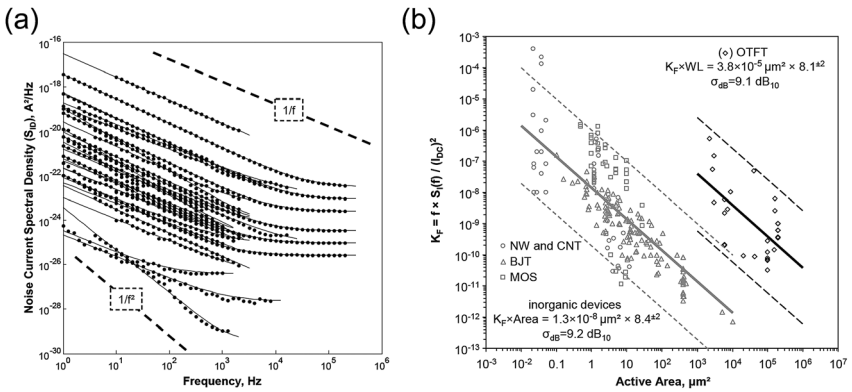

Fig. 7 Distribution of noise spectra of OTFTs. (a) Noise spectra of OTFTs. Symbols denote published data. Thin curves denote approximation $S_{ID}(1\text{ Hz})/f + S_{white}$. (b) Normalized low frequency noise, $f \cdot S_{ID}/I_D^2 \propto K_F$, is the reciprocal function of the channel area $W \cdot L$ in OTFTs and inorganic TFTs. Reproduced with permission from ref. 65, Copyright 2015, IEEE.

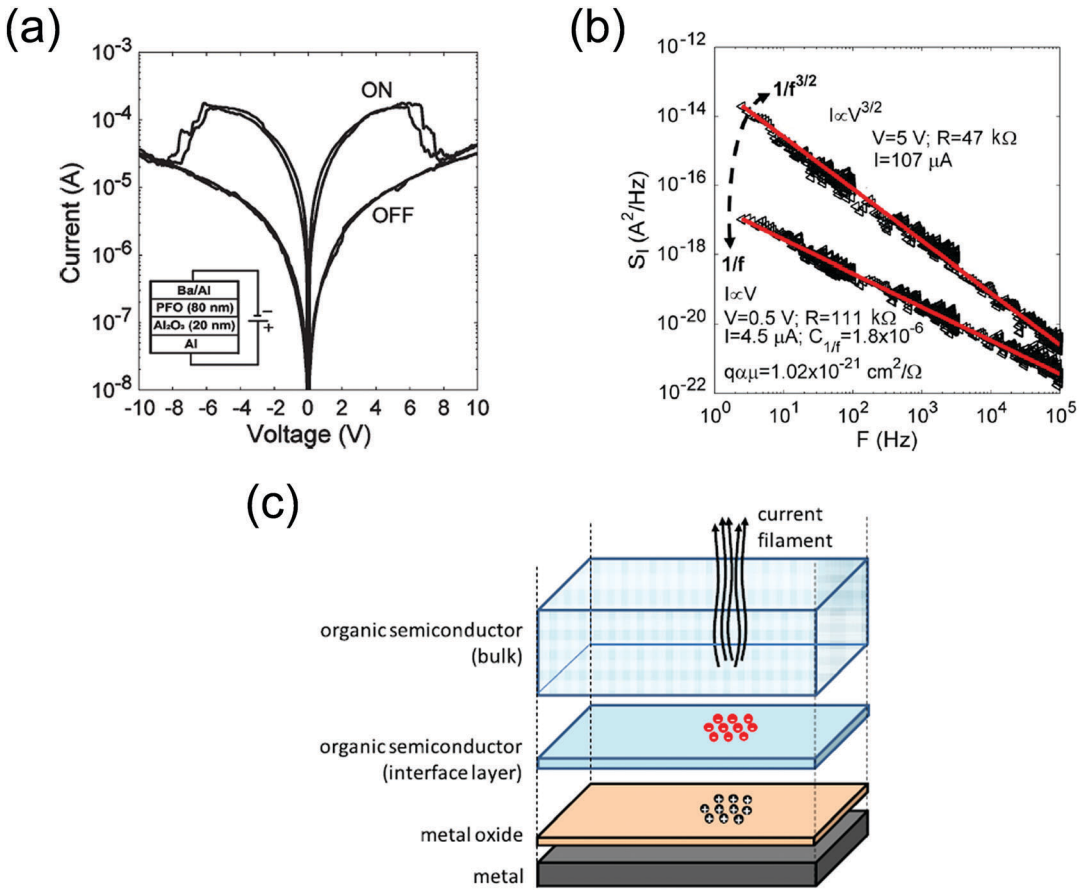

Fig. 8 *I–V* and noise characteristics of the metal-oxide polymer resistive memory device. (a) *I–V* characteristics in the ON and OFF states of an Al/Al_2O_3/PFO/Ba/Al bistable resistive-switching diode. The inset shows the device structure. (b) Current noise spectrum in the transition from the ohmic to SCL region, indicating a diffusion mechanism at higher bias. (c) Schematic representation of a current filament. Reproduced with permission: (a) and (b) from ref. 67, Copyright 2012, IEEE; and (c) from ref. 69, Copyright 2015, AIP Publishing LLC.

3.2.2. Organic nanocomposite resistive memory devices. Organic resistive memory devices using blends of conducting/semiconducting molecules and insulating polymers have exhibited high device quality, high on/off ratios, enhanced endurance properties and stable memory characteristics under thermal stress.[6,136,137] This type of organic resistive memory can be considered as a nanocomposite system because conductive nanoclusters/molecules are embedded in the insulating polymer, forming a highly disordered electronic structure. The switching mechanism of organic nanocomposite resistive memory devices has been debated, and Coulomb blockade conduction,[137] metal filament formation,[138] and trap-filling conduction[139] have been suggested. Many nanocomposite resistive memory devices have shown multistorage functionality, such as intermediate resistive states (IRSs) that are found between the highest resistive state (HRS) and the lowest resistive state (LRS).

Song *et al.* proposed advanced insights into the switching mechanism of nanocomposite resistive memory devices *via* a noise analysis.[70] Fig. 9a shows the unipolar switching characteristics of polyimide:phenyl-C61-butyric acid methyl ester (PI:PCBM) resistive memory devices. By applying voltage sweeps with different V_{end} values (5.5 V to 10 V) at the NDR of each sweep, various IRSs could be approached. Typically, when the V_{end} value was higher, the current level became lower (higher resistive state). In addition, the S_I/I^2 spectra were measured at the LRS, HRS and NDR, which exhibited $1/f^{\gamma}$ noise with $\gamma = 1$ for the HRS and LRS and $\gamma = 1.5$ for the NDR (Fig. 9b). The exponent value increased from 1 to 1.5 gradually as the applied bias increased from 1 V. The increase in γ from low bias to high bias indicated different dominant charge transport behavior in the NDR (Fig. 9c). Meanwhile, at low biases (0.5 V), all the IRSs, including the HRS and LRS, showed $\gamma = 1$, with increasing relative noise amplitude as the resistance increased. The relation between the relative noise and resistance of the IRS exhibited a power-law ($S_I/I^2 \propto R^{\omega}$) with $\omega = 0.95$ (Fig. 9d). This scaling behavior indicated the percolative formation of localized current pathways as the origin of the IRSs. However, the physical nature of the localized current pathways was still not clear. One possibility was metal conductive filament formation caused by metal ion migration from the electrodes. However, unipolar *I–V* characteristics were observed despite the asymmetric electrode structure (Al/PI:PCBM/Au), and the nonohmic behavior at all IRSs, even for the LRS ($\sim$1 kΩ), denied the possibility of metal conductive filament formation.[70] Note that another noise scaling behavior with $\omega = 1.8$ was reported for a NiO resistive memory device in which Ni metal filament formation occurred.[140] Song *et al.* argued that a trapping–detrapping process could explain

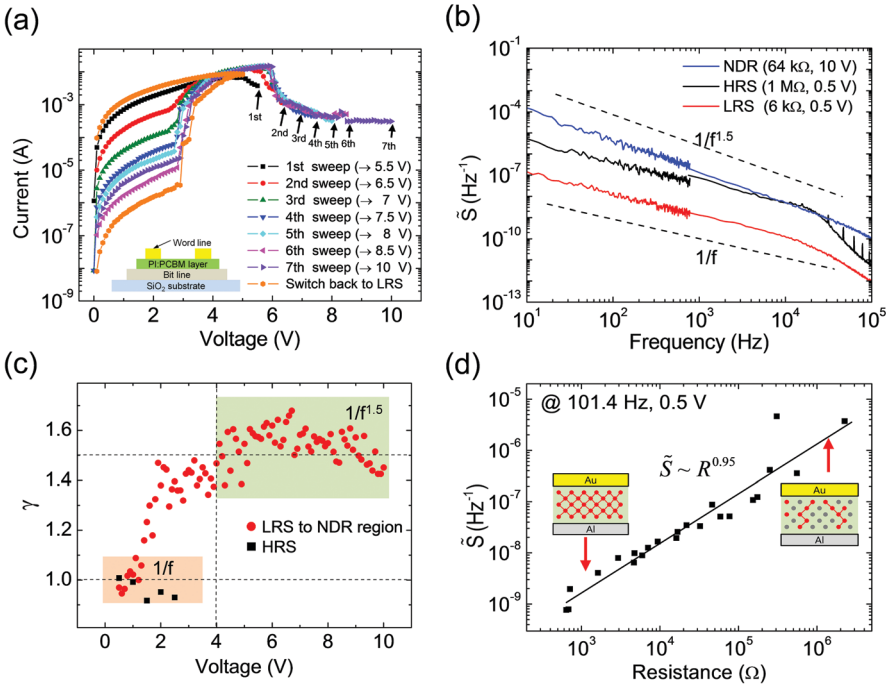

Fig. 9 *I–V* and noise characteristics of the organic nanocomposite resistive memory. (a) *I–V* characteristics of PI:PCBM memory devices exhibiting multiple current levels. (b) Relative current noise power spectral densities of the LRS, HRS, and NDR. (c) The values of the γ (at $S_I \sim 1/f^{\gamma}$) from the LRS to NDR change from 1 to 1.5. (d) Power-law relationship between the relative noise and the resistance of the IRSs, at f = 101.4 Hz and 0.5 V bias. Reproduced with permission from ref. 70, Copyright 2015, American Chemical Society.

the nature of the localized current pathways. They also reported telegraphic noise at the NDR characterized by long characteristic times (tens of milliseconds). They suggested that PI:PCBM had a distribution of deep trap levels, and charge trapping/detrapping processes at the deep trap levels were the source of the telegraphic noise and percolation behavior.

Song *et al.* further studied the noise characteristics of other organic nanocomposite memory (polystyrene:PCBM (PS:PCBM)) devices under variable temperature conditions.[71] In their study, they measured noise spectra at 100 K, 200 K, and 300 K, and then observed the temperature dependence of the noise characteristics. Specifically, time traces showed that the telegraphic noise at the NDR (at 8 V) was drastically reduced and showed longer dwell times at 200 K and 100 K (Fig. 10a). The telegraphic noise also showed reversible transitions between more than two current states, as clearly shown at 6 V and 200 K (Fig. 10b). If the telegraphic noise was related to the diffusion of the filamentary element, the current level would not have been reversibly accessible. The reversible access of the current levels indicated that telegraphic noise occurred in the stationary structures, such as localized traps. They concluded that this telegraphic noise could be understood as current path fluctuations induced by charge trapping and detrapping in the deep trap levels distributed in the organic nanocomposite memory device. Fig. 10c illustrates this argument. The white boxes indicate the gap between the lowest unoccupied molecular orbital (LUMO) and the highest occupied molecular orbital (HOMO) of the insulating matrix (PS or PI). Charge carriers can be trapped and localized in the deep trap energy levels due to a high trap-energy barrier relative to the conduction level of the insulating matrix. If deep trap levels are already occupied by charge carriers, charge carriers can easily pass through the shallow trap levels above the deep trap levels *via* trap-assisted tunneling or the Poole–Frenkel conduction process. Hence, IRSs can be understood as the localized current pathways formed by deeply occupied traps as a result of V_{end} modulation in the NDR regime. The PS:PCBM memory device also showed noise scaling behavior similar to PI:PCBM with ω = 1.27 at room temperature, as expected. The ω value decreased from 1.27 to 0.88 as the temperature decreased from 300 K to 80 K (Fig. 10d). The change in ω was attributed to the geometrical variations in the current pathways.

3.3. Noise analyses on molecular-scale electronic devices

In this section, we discuss noise studies on molecular-scale electronic devices, in which molecules represent ultimate downscaled organic materials.[141,142] Metal/molecules/metal junctions are highly sensitive to the interfacial formation of traps or their configurational changes when their electric currents are measured.[143] The dynamics of trapping/detrapping during trap or redox events could be observed as RTNs in SAM junctions. In the case of single-molecule junctions, the configurational change and the charge transmission characteristics of the molecular junction were analyzed through electronic noise measurements.

3.3.1. Self-assembled monolayer (SAM) junctions. Kim *et al.* observed RTN signals in their metal–molecule–metal junctions, demonstrating the existence of localized traps in the molecular junctions.[72] They used SAM-based molecular junctions in which

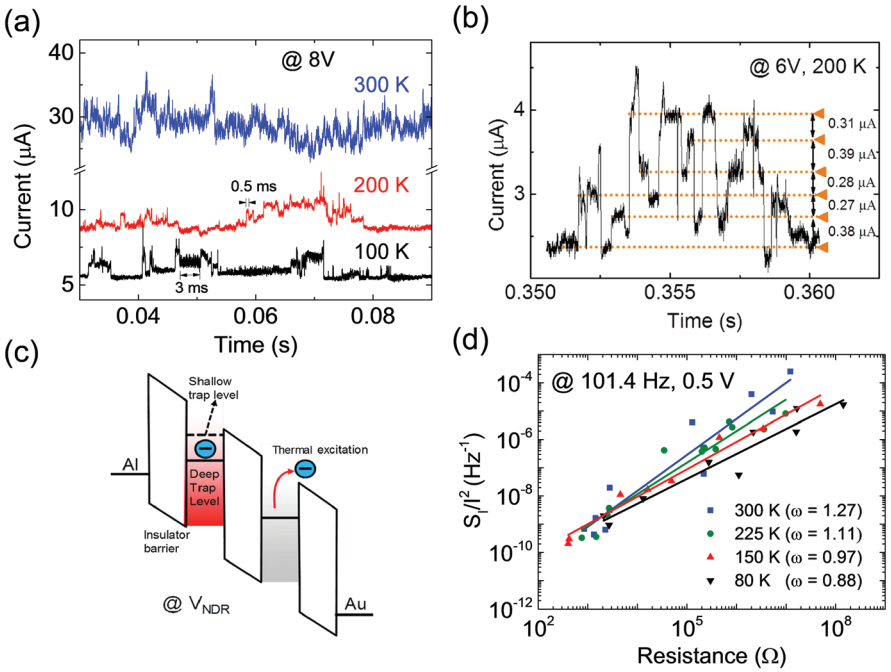

Fig. 10 Current noises of PS:PCBM memory devices under different temperature conditions. (a) Time traces of currents at 100 K, 200 K, and 300 K in the NDR regime (8 V bias) for 50 ms. (b) Well-separated current plateaus at 6 V bias and 200 K. (c) Schematic of the current pathway removal process with NDR modulation. The blue colored circles indicate the electrons that are localized in the deep trap levels or escaping the deep trap levels. (d) Power-law relationships between the relative power spectral densities and the resistance of the IRSs at 80 K, 150 K, 225 K, and 300 K with f = 101.4 Hz and 0.5 V bias. Reproduced with permission from ref. 71, Copyright 2016, Macmillan Publishers Limited, part of Springer Nature.

1,6-hexanedithiol (HDT) molecules were self-assembled between Au electrodes (Fig. 11a). They noted that the defective molecular junctions (4%, 16 devices of the 400 devices) exhibited peculiar and consistent noise behavior that was different from the normal devices. The noise spectra of the defective molecular junctions exhibited $1/f$ noise behavior under 20 Hz and $1/f^2$ noise behavior above 20 Hz, indicating a superposition of different noise sources, while the normal devices only exhibited $1/f$ noise (Fig. 11b). The relative noise amplitude showed a local bump at 0.6 V. In addition, they observed a local bump in the relative noise amplitude at approximately 0.6 V, which was absent in the normal devices. These behaviors indicated the localization of defects in the molecular junction. Furthermore, voltage-dependent RTN signals were observed in the defective devices (Fig. 11c and d). The RTN signals with two-level current fluctuations could be modulated by the voltage bias, and a higher voltage bias led to a longer dwelling time at the high current level. The fluctuations between the two-current levels could be explained as the localization of charge carriers at the trap states in the molecular junction. When a charge carrier was in the trapped state or detrapped state, low or high current levels were observed, respectively. The applied voltage could modulate the potential difference between the trapped state and conduction level of the metal; hence, higher voltage biases induced higher rates of re-emission from the trapped state (Fig. 11e).

Arielly *et al.* observed the redox events in SAM-based molecular junctions.[73] The molecular junctions had a suspended Au nanowire that was covered with thiol molecules, as seen in Fig. 12a. The self-assembled mixed-monolayer-covered Au nanowires consisted of 1-dodecanethiol (denoted C12) and 6-(ferrocenyl)hexanethiol (FHT) molecules at a ratio of 3 : 1. The SAM-treated Au nanowires could be suspended onto bottom Au leads using a dielectrophoresis technique. FHT molecules have ferrocene groups in which oxidation–reduction reactions can easily occur due to an applied electric field.[16] The FHT molecules were diluted with C12 molecules to establish weak coupling interactions with the second Au electrode and to ensure sufficient time for structural rearrangement during the charging events (Fig. 12b). Applying a DC voltage at the junction at a low temperature (77 K), they observed voltage-dependent two-level fluctuation (TLF) of the current level with a long characteristic time (milliseconds). The TLF behavior was observed only in the molecular junctions with the FHT molecules, while the other SAM junctions with alkanes of various lengths, such as 1,1′,4′,1″-terphenyl-4-thiol, biphenyl-4,4′-dithiol, and various oligophenylene ethynylenes, did not exhibit TLF behavior. Therefore, junction conductivity fluctuations due to the stochastic process of oxidation–reduction in the FHT molecules were suggested as the cause of the TLF behavior. The voltage-dependent rates of oxidation and reduction were formulated and fitted to the experimental data. The extracted parameters such as the reorganization energy, energy level alignment, and transition probability were in good agreement with the reported values. The possible mechanism for the varying conductance with the different redox states can be explained by two factors. (a) The redox state could affect the conductivity of the neighboring C12 molecules by shifting the LUMO of the C12 molecules. (b) The conductivity of the FHT molecules themselves could change due to the

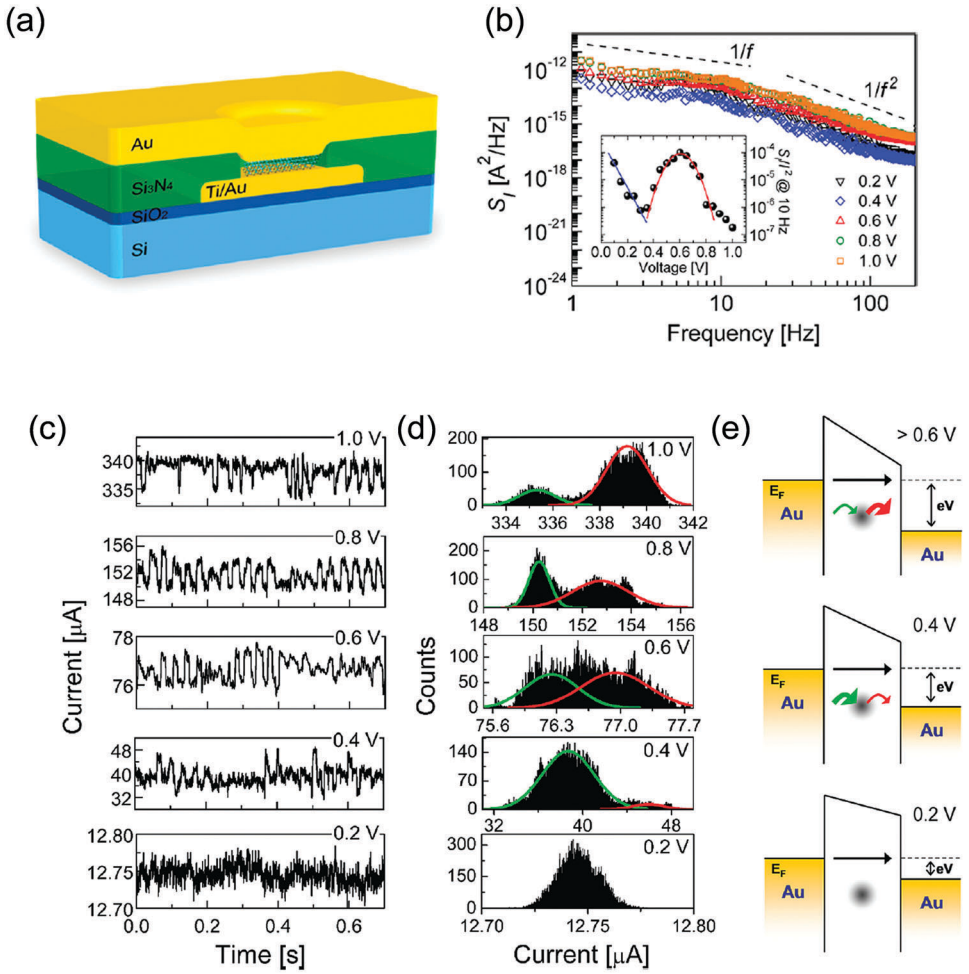

Fig. 11 Noise characteristics of a molecular junction with a single localized trap. (a) Schematic diagram of the molecular device structure with a molecular structure of hexanedithiol (HDT). (b) Low frequency power current noise spectra of the Au–HDT–Au junction. The inset shows the voltage dependence of the relative power spectrum of current noise at frequency f = 10 Hz, indicating a localization of defects. (c) Time-dependent two-level RTNs of the Au–HDT–Au junction (3 μs per point at room temperature for 0.7 s). (d) Corresponding histograms for the RTNs. The histograms are fitted with Gaussian peaks where green and red lines indicate trapping and detrapping events, respectively. (e) Schematic energy band diagrams of the molecular junction with a single localized trap. Reproduced with permission from ref. 72, Copyright 2010, American Chemical Society.

HOMO–LUMO gap change. The existence of only two-level fluctuation of currents could not be obviously explained in this study. The number of FHT molecules in the junction was estimated to be approximately 3000. Therefore, if each FHT molecule underwent the redox process independently, the resultant current fluctuation would not show TLFs due to superposition. If patches of the FHT molecules underwent redox processes coherently due to attractive interactions between adjacent molecules or only single FHT molecules participated in the redox process, TLFs would be observed.

3.3.2. Single-molecule junctions. Single-molecule junctions are well-defined structures to be studied for engineering extremely downsized OEDs.[141] Xiang *et al.* observed telegraphic noise and Lorentzian-shaped $1/f^2$ noise in their organic single-molecule junctions.[74,75] The single-molecule junctions were characterized using mechanically controllable break junctions (MCBJs) (Fig. 13a). 1,8-Octanedithiol (ODT), 1,4-benzenedithiol (BDT), and 11-mercaptoundecanoic acid (MUA) were used to study the noise properties at room temperature. The anchoring of a single molecule could be identified by measuring the conductance of the lock-in state while increasing the push rod displacement.[75] For example, the conductance of the BDT junction was measured to be approximately $6 \times 10^{-3} G_0$, where G_0 is the conductance quantum ($2e^2/h$). Without molecules in the MCBJ, the tunneling current through the junction showed $1/f$-type noises. The noise amplitudes were varied by varying the junction gap size, showing that the noise amplitude was quadratically dependent on the current level ($S_I \propto I^2$) (Fig. 13b). When a molecule was anchored in the junction, the noise spectra showed extra $1/f^2$ components. All the molecular junctions in this study showed Lorentzian noise with different characteristic frequencies (f_0) (Fig. 13c). The f_0 values were found to be 1.1 kHz for BDT, 0.27 kHz for ODT and 0.07 kHz for the MUA molecules at a 20 mV bias. The f_0 values were not

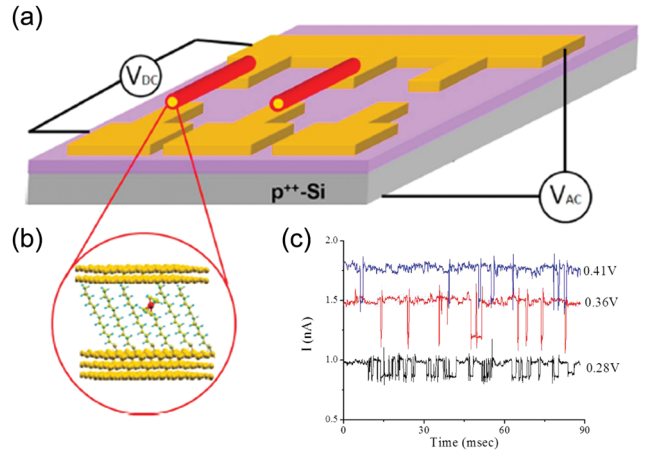

Fig. 12 Detection of redox events in ferrocene-based molecular junctions. (a) Schematics of monolayer-covered Au nanowires suspended on lithography defined Au contact pads on top of an oxide covered Si substrate. Alignment of nanowires is achieved by dielectrophoresis using an AC voltage, V_{AC}. Measurement of a certain junction is performed by applying a DC voltage, V_{DC}, between the common pad and the relevant floating pad. (b) Schematics of a part of a mixed monolayer with one (ferrocenyl)hexanethiol (FHT) molecule and diluting thiol–alkyl chains. The ferrocene group is coupled to one side of the junction *via* an alkyl chain, and to the other *via* space. (c) Current–time traces showing two-level fluctuation (TLF) signals. Reproduced with permission from ref. 73, Copyright 2014, American Chemical Society.

dependent on the bond strength or atomic bonding type with the electrode. Therefore, the induced telegraphic noise could not have originated from the contact between the molecules and the electrode, but rather most likely originated from the molecular structure. In the time domain, telegraphic noise was observed in the single-molecule junctions, while the vacuum junctions did not exhibit telegraphic noise (Fig. 13d). The small difference (1.5 nA, 12% of the current level) between the high and low current levels also excluded the possibility of the interfacial contact effect, in which breakage and reconnection of molecules at the bonding interface can occur. The slow characteristic times were attributed to the slow processes induced by the structural or configurational changes in the molecule due to the correlation between charge transfer through a molecular junction and structural changes. The molecular changes induced by the channel current were compared using a Lorentz oscillator in which Lorentzian noise could be induced. Supporting this argument, they found a consistent dependence of f_0 on the current level and molecular weight ($f_0 \propto I, f_0 \propto M^{-1/2}$, where M denotes the molar mass of a molecule).

The conductance values measured for the same single-molecule junctions have been widely spread because of the junction geometry.[76–78] In this regard, single-molecule junctions fabricated using an MCBJ can realize a mesoscopic system in which one-dimensional electrons can be transported through narrow constrictions between two electrodes (so called quantum point contacts). A shot noise analysis can provide essential information on molecular junctions, such as the effective number of channels, the transmission/reflection rates of an electron at the junction, and the degree of correlation between the tunneling

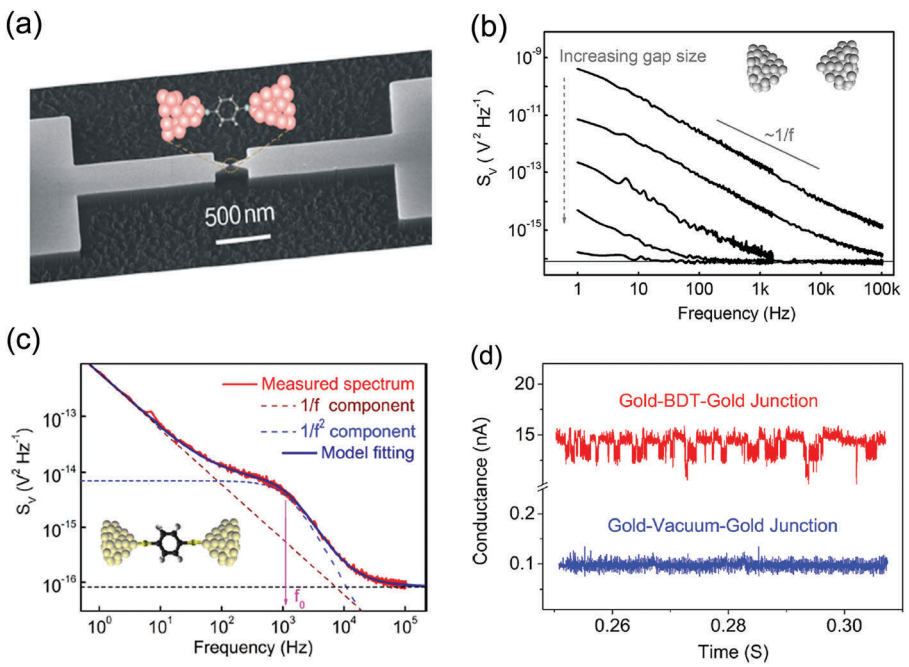

Fig. 13 Noise characteristics of single-molecular junctions. (a) Scanning electron microscopy image of a nanofabricated mechanically controllable break junction (MCBJ). Inset: Schematic drawing of two nano-electrodes bridged by a molecule (1,4-benzenedithiol (BDT)). (b) The voltage noise power spectral density of the molecule-free junctions in the tunneling regime, measured with respect to different gap sizes between the gold nanoelectrodes. The tunneling resistance is measured to be 0.022, 0.030, 0.170, 1, and 10 MΩ from top to bottom, respectively. (c) The noise power spectral density of the molecule containing junction in the lock-in state for a single BDT molecule bridging two electrodes. Reproduced with permission: (a), (c) and (d) from ref. 74, Copyright 2015, AIP Publishing LLC; and (b) from ref. 75, Copyright 2012, AIP Publishing LLC.

charges. A full expression for the noise level of a quantum point contact with N channels can be expressed as:[77,80,144]

$$S_I = 2qV\coth\left(\frac{qV}{2k_BT}\right)\frac{2q^2}{h}\sum_i^N \tau_i(1-\tau_i) + 4k_BT\frac{2q^2}{h}\sum_i^N \tau_i^2 \quad (11)$$

where k_BT is the thermal energy, h is the Planck constant, and τ_i is the transmission probability of the i-th channel. The left term indicates the shot noise, and the right term indicates the thermal noise. For $k_BT \ll qV$, eqn (11) reduces to $S_I = 2q|\bar{I}|F$, where $\bar{I}$ is the average current over time and F is the Fano factor given as:

$$F = \frac{\sum_i^N \tau_i(1-\tau_i)}{\sum_i^N \tau_i} \quad (12)$$

After fitting the Fano factor with the actual shot noise level, one can obtain useful information about the number of channels (N) and transmission probabilities (τ_i). Therefore, by measuring the shot noise, one can gain insights into the microscopic details of a mesoscopic system (note that the uncertainty in the fitted values (N and τ_i) is very small since the fitting is sensitive to N and τ_i). The first shot noise measurements were performed by Ruitenbeek *et al.* using a single deuterium molecule device at a cryogenic temperature (4 K).[144] They found that the shot noise was suppressed ($F \sim 0.02$) with $G \sim G_0$ in the device. This result indicated that their deuterium-molecule junction was almost transparent, with a transmission probability of $\sim$0.995. A single channel seemed to dominate because additional channels gave very small transmission probabilities ($\tau_i < 0.01$, $i \neq 1$). Organic molecules have complex structures, and junction geometries can be numerous according to the junction size and bonding sites, leading to widely spread conductance values and various channel numbers. For shot noise measurements of organic single-molecule junctions, Ruitenbeek *et al.* showed that Pt–benzene–Pt junctions without any anchoring groups could have different channel numbers and transmission probabilities according to the various junction geometries with different junction conductivities.[76] Recently, Sheer *et al.* analyzed the shot noise of Au–BDT–Au junctions with Au–S binding by employing a similar shot noise analysis by Ruitenbeek *et al.*[77] They used well-defined single-molecule junctions, which were identified by the vibration mode peaks in their inelastic electron tunneling spectra and symmetrical binding at the electrodes using *I–V* fitting. They measured the shot noise on molecular junctions with a conductance range from low ($G \sim 10^{-2}G_0$) to high ($G > 0.1G_0$). From the shot noise measurements on the molecular junctions ($0.23G_0$) at the cryogenic temperature (4.2 K), a single-channel assumption provided the best fitting result for the shot noise level and applied voltage functions (Fig. 14a). The fitted value of the transmission probability was 0.23, which corresponded to the Landauer formula ($G = \tau G_0$ for a single channel). As shown in Fig. 14b, multiple channels produced incorrect fitting results that were higher than the actual data. The X and Y at each axis indicate the expressions of the applied voltage and shot noise level for the simplified fitting, respectively. The single-channel fitting also correlated the best with the other molecular devices with lower conductance values down to $0.037G_0$, although the contribution of additional channels could not be ignored at low conductance values. These results indicate that a single conduction channel dominated the transport for most of the electrode separations. The single-channel formation was also identified from the junction geometry investigation using density functional calculations while increasing the channel lengths (Fig. 14c).

4. Summary and outlook

Organic electronic devices (OEDs) have been extensively studied for various device applications with fast-paced progress. While research on organic electronic devices has often focused on trial-based optimization of the device performance, a precise understanding of organic electronic devices has been overlooked because of the unpredictable and disordered structure of the utilized organic materials. Noise analyses can provide not only a figure of merit for OEDs but also statistical information and deep insights into the intrinsic nature of OEDs. In this review, various noise analyses on OEDs, including organic thin film transistors, organic resistive memory devices, and molecular junction devices, were explored for characterizing the fluctuation responses and device physics. In the case of bulk organic materials, the major factors that affect the noise characteristics are the trap distribution inside the organic material and the interfacial morphology. Due to their highly disordered structures, OEDs show generally large noise amplitudes compared to crystallized inorganic devices. In the case of molecular junction devices, small changes in the molecules, such as single-trap formation and chemical and conformational changes, can exhibit huge noise signal differences, such as random telegraphic noise or Lorentzian noise due to the subnanometer junction scale. Shot noise measurements in single-molecule junctions can provide profound information about the tunneling characteristics, such as the tunneling rate and number of tunneling channels.

There are many challenges to be resolved regarding the electronic noise characteristics of OEDs. While there may be other crucial issues, we think that the following issues are the essential research areas. (i) Downscaling issues – because the noise amplitude is generally high in OEDs, the sensitivity of future OEDs with downscaled and highly integrated electronic circuits will be seriously determined by the noise. The contact, crystallinity, and trap formation will be the important factors affecting the high noise levels in downscaled OEDs. Therefore, it will be valuable to accomplish low-noise generating OEDs by controlling such factors. (ii) Disorder and trap issues: disorder and trap formation in OEDs are the crucial contributors for noise generation. However, it seems that studies regarding systemic noise analyses on the relation between the microscopic arrangement of organic materials and noise generation do not exist. Organic semiconducting polymers exhibit different

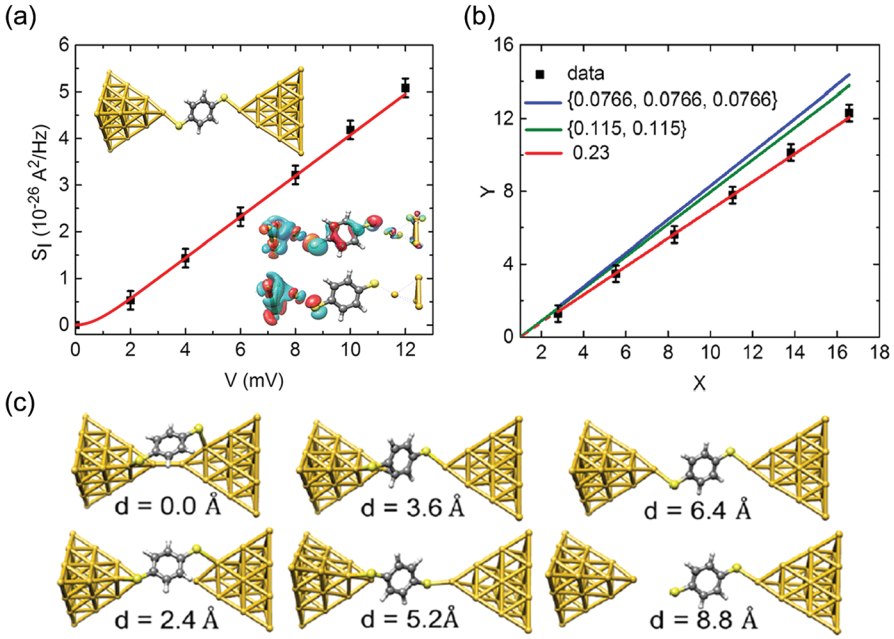

Fig. 14 Shot noise measured from single-molecular junctions at 4.2 K. (a) Shot noise as a function of the bias voltage applied across the Au–BDT–Au junction. The zero-bias conductance for this junction is $0.23G_0$. The red line is the fit to eqn (11), yielding a transmission probability of $\tau_1 = 0.23$. (b) The excess noise, plotted for the reduced parameters X and Y. The red line is the fit to the data and gives a Fano factor of $F = 0.77$ for $\tau_1 = 0.23$. The green line is the calculated excess noise for two channels with the same transmission probabilities of $\tau_1 = \tau_2 = 0.115$ and the blue line is those for three channels with $\tau_1 = \tau_2 = \tau_3 = 0.0766$. (c) Junction geometries at selected stages of the stretching process. Reproduced with permission from ref. 77, Copyright 2016 American Chemical Society.

microscopic orders and mobilities according to their molecular weight (molecular length).[145,146] Organic blends of thin films are known to exhibit reduced trap formation.[30] Furthermore, it is known that one can reduce the noise of organic photodiodes by trap-controlled engineering, in which electric noise in dark current is highly important for enhancing photo-sensitivity.[147–150] Therefore, noise analyses on such organic systems or other variable systems would provide meaningful insights regarding the microscopic details of the organic material system. (iii) Noise analyses on functional molecular junctions: specifically, single-molecule junctions with functionality show interesting noise phenomena. For example, diarylethene molecules are known to change their molecular structures in response to UV and visible light, showing different conduction properties in each molecular state.[151] In diarylethene molecular junctions, the transmission probability varies according to the molecular state; hence, such junctions may exhibit shot noise characteristics with the molecular state. It would also be worth analyzing the noise characteristics of gate-biased single-molecule junctions,[152] in which external fields can modulate the electronic structures of the molecules in the junction.

The most attractive property of OEDs is the tremendous variability in their electronic functionality, which can be modulated using extensive chemical compositions from simple carbon dioxide to complex biopolymers and arrangements of organic molecules/polymers. Noise analyses on OEDs in the past decade have provided considerable insights into the variability of OEDs, regarding the microscopic and statistical comprehension of their charge transport and electronic structures. In many cases, noise analyses alone cannot provide decisive information for the target sample. However, a noise analysis is greatly effective when it is compared with and supported by other analysis methods such as current–voltage characterization studies, morphological analyses, and spectroscopic analyses. Finally, based on the presented interpretations of the noise phenomena of OEDs in this review, we think that noise analyses can yield more meaningful insights into the conducting phenomena of various OEDs.

Acknowledgements

The authors appreciate the financial support of the National Creative Research Laboratory program (Grant No. 2012026372) through the National Research Foundation of Korea (NRF).

References

1 B. C.-K. Tee, A. Chortos, A. Berndt, A. K. Nguyen, A. Tom, A. McGuire, Z. C. Lin, K. Tien, W.-G. Bae, H. Wang, P. Mei, H.-H. Chou, B. Cui, K. Deisseroth, T. N. Ng and Z. Bao, *Science*, 2015, **350**, 313–316.
2 J. You, L. Dou, K. Yoshimura, T. Kato, K. Ohya, T. Moriarty, K. Emery, C.-C. Chen, J. Gao, G. Li and Y. Yang, *Nat. Commun.*, 2013, **4**, 1446.
3 Y. Zhao, C.-A. Di, X. Gao, Y. Hu, Y. Guo, L. Zhang, Y. Liu, J. Wang, W. Hu and D. Zhu, *Adv. Mater.*, 2011, **23**, 2448–2453.

4 J. Ouyang, C.-W. Chu, C. R. Szmanda, L. Ma and Y. Yang, *Nat. Mater.*, 2004, **3**, 918–922.
5 S. Savagatrup, E. Chan, S. M. Renteria-Garcia, A. D. Printz, A. V. Zaretski, T. F. O'Connor, D. Rodriquez, E. Valle and D. J. Lipomi, *Adv. Funct. Mater.*, 2015, **25**, 427–436.
6 Y. Ji, D. F. Zeigler, D. S. Lee, H. Choi, A. K.-Y. Jen, H. C. Ko and T.-W. Kim, *Nat. Commun.*, 2013, **4**, 2707.
7 S. R. Forrest, *Nature*, 2004, **428**, 911–918.
8 C. D. Dimitrakopoulos and D. J. Mascaro, *IBM J. Res. Dev.*, 2001, **45**, 11–27.
9 T. Someya, Y. Kato, T. Sekitani, S. Iba, Y. Noguchi, Y. Murase, H. Kawaguchi and T. Sakurai, *Proc. Natl. Acad. Sci. U. S. A.*, 2005, **102**, 12321–12325.
10 T. Sekitani and T. Someya, *Adv. Mater.*, 2010, **22**, 2228–2246.
11 M. Muccini, *Nat. Mater.*, 2006, **5**, 605–613.
12 A. L. Briseno, S. C. B. Mannsfeld, M. M. Ling, S. Liu, R. J. Tseng, C. Reese, M. E. Roberts, Y. Yang, F. Wudl and Z. Bao, *Nature*, 2006, **444**, 913–917.
13 H. T. Yi, M. M. Payne, J. E. Anthony and V. Podzorov, *Nat. Commun.*, 2012, **3**, 1259.
14 Y.-Y. Noh, N. I. Zhao, M. Caironi and H. Sirringhaus, *Nat. Nanotechnol.*, 2007, **2**, 784–789.
15 H. Yan, Z. Chen, Y. Zheng, C. Newman, J. R. Quinn, F. Dötz, M. Kastler and A. Facchetti, *Nature*, 2009, **457**, 679–686.
16 H. Jeong, D. Kim, G. Wang, S. Park, H. Lee, K. Cho, W.-T. Hwang, M.-H. Yoon, Y. H. Jang, H. Song, D. Xiang and T. Lee, *Adv. Funct. Mater.*, 2014, **24**, 2472–2480.
17 S. Park, G. Wang, B. Cho, Y. Kim, S. Song, Y. Ji, M.-H. Yoon and T. Lee, *Nat. Nanotechnol.*, 2012, **7**, 438–442.
18 G. Gu, M. G. Kane, J. E. Doty and A. H. Firester, *Appl. Phys. Lett.*, 2005, **87**, 243512.
19 R. Noriega, J. Rivnay, K. Vandewal, F. P. V. Koch, N. Stingelin, P. Smith, M. F. Toney and A. Salleo, *Nat. Mater.*, 2013, **12**, 1038–1044.
20 S. Wang, S. Fabiano, S. Himmelberger, S. Puzinas, X. Crispin, A. Salleo and M. Berggren, *Proc. Natl. Acad. Sci. U. S. A.*, 2015, **112**, 10599–10604.
21 H. Peisert, T. Schwieger, J. M. Auerhammer, M. Knupfer, M. S. Golden, J. Fink, P. R. Bressler and M. Mast, *J. Appl. Phys.*, 2001, **90**, 466–469.
22 A. Ojala, H. Bürckstümmer, J. Hwang, K. Graf, B. von Vacano, K. Meerholz, P. Erk and F. Würthner, *J. Mater. Chem.*, 2012, **22**, 4473–4482.
23 D. P. McMahon and A. Troisi, *ChemPhysChem*, 2010, **11**, 2067–2074.
24 H. Sirringhaus, *Adv. Mater.*, 2005, **17**, 2411–2425.
25 T. Richards, M. Bird and H. Sirringhaus, *J. Chem. Phys.*, 2008, **128**, 234905.
26 V. Coropceanu, J. Cornil, D. A. da Silva, Y. Olivier, R. Silbey, J.-L. Brédas, D. A. da Silva Filho, J.-L. Brédas, Y. Olivier, R. Silbey and J.-L. Brédas, *Chem. Rev.*, 2007, **107**, 926–952.
27 A. Ulman, *Chem. Rev.*, 1996, **96**, 1533–1554.
28 J. C. Love, L. A. Estroff, J. K. Kriebel, R. G. Nuzzo and G. M. Whitesides, *Chem. Rev.*, 2005, **105**, 1103–1169.
29 R. Schmechel and H. von Seggern, *Phys. Status Solidi A*, 2004, **201**, 1215–1235.
30 D. Abbaszadeh, A. Kunz, G. A. H. Wetzelaer, J. J. Michels, N. I. Crăciun, K. Koynov, I. Lieberwirth and P. W. M. Blom, *Nat. Mater.*, 2016, **15**, 628–633.
31 J. Sworakowski and K. Pigoń, *J. Phys. Chem. Solids*, 1969, **30**, 491–496.
32 L. D. Bozano, B. W. Kean, M. Beinhoff, K. R. Carter, P. M. Rice and J. C. Scott, *Adv. Funct. Mater.*, 2005, **15**, 1933–1939.
33 J. Dacuña and A. Salleo, *Phys. Rev. B: Condens. Matter Mater. Phys.*, 2011, **84**, 195209.
34 S. Olthof, S. Mehraeen, S. K. Mohapatra, S. Barlow, V. Coropceanu, J.-L. Brédas, S. R. Marder and A. Kahn, *Phys. Rev. Lett.*, 2012, **109**, 176601.
35 L. K. J. Vandamme, R. Feyaerts, G. Trefán and C. Detcheverry, *J. Appl. Phys.*, 2002, **91**, 719–723.
36 J.-H. Kwon, M.-H. Chung, T.-Y. Oh, B.-K. Ju and F. Yakuphanoglu, *Microelectron. Eng.*, 2010, **87**, 2306–2311.
37 B. Gunduz and F. Yakuphanoglu, *Sens. Actuators, A*, 2012, **178**, 141–153.
38 B. R. Conrad, W. G. Cullen, W. Yan and E. D. Williams, *Appl. Phys. Lett.*, 2007, **91**, 242110.
39 O. D. Jurchescu, B. H. Hamadani, H. D. Xiong, S. K. Park, S. Subramanian, N. M. Zimmerman, J. E. Anthony, T. N. Jackson and D. J. Gundlach, *Appl. Phys. Lett.*, 2008, **92**, 132103.
40 Z. Jia, I. Meric, K. L. Shepard and I. Kymissis, *IEEE Electron Device Lett.*, 2010, **31**, 1050–1052.
41 M. Jamal Deen, O. Marinov, J. Yu, S. Holdcroft and W. Woods, *IEEE Trans. Electron Devices*, 2001, **48**, 1688–1694.
42 O. Marinov, M. J. Deen, J. Yu, G. Vamvounis, S. Holdcroft and W. Woods, *IEE Proc.-Circuits Devices Syst.*, 2004, **151**, 466–472.
43 S. Martin, A. Dodabalapur, Z. Bao, B. Crone, H. E. Katz, W. Li, A. Passner and J. A. Rogers, *J. Appl. Phys.*, 2000, **87**, 3381–3385.
44 L. Ke, S. B. Dolmanan, L. Shen, C. Vijila, S. J. Chua, R.-Q. Png, P.-J. Chia, L.-L. Chua and P. K.-H. Ho, *J. Appl. Phys.*, 2008, **104**, 124502.
45 H. Kang, L. Jagannathan and V. Subramanian, *Appl. Phys. Lett.*, 2011, **99**, 062106.
46 H. Kang and V. Subramanian, *Appl. Phys. Lett.*, 2014, **104**, 023301.
47 R. Ruiz, A. Papadimitratos, A. C. Mayer and G. G. Malliaras, *Adv. Mater.*, 2005, **17**, 1795–1798.
48 A. Dodabalapur, L. Torsi and H. E. Katz, *Science*, 1995, **268**, 270–271.
49 G. Giusi, O. Giordano, G. Scandurra, S. Calvi, G. Fortunato, M. Rapisarda, L. Mariucci and C. Ciofi, *IEEE Trans. Electron Devices*, 2016, **63**, 1239–1245.
50 G. Giusi, O. Giordano, G. Scandurra, S. Calvi, G. Fortunato, M. Rapisarda, L. Mariucci and C. Ciofi, *IEEE Electron Device Lett.*, 2015, **36**, 390–392.
51 D. Gupta, M. Katiyar and D. Gupta, *Org. Electron.*, 2009, **10**, 775–784.
52 I. Kymissis, C. D. Dimitrakopoulos and S. Purushothaman, *IEEE Trans. Electron Devices*, 2001, **48**, 1060–1064.

53 P. V. Necliudov, S. L. Rumyantsev, M. S. Shur, D. J. Gundlach and T. N. Jackson, *J. Appl. Phys.*, 2000, **88**, 5395–5399.
54 A. D. Carlo, F. Piacenza, A. Bolognesi, B. Stadlober and H. Maresch, *Appl. Phys. Lett.*, 2005, **86**, 263501.
55 S. Verlaak and P. Heremans, *Phys. Rev. B: Condens. Matter Mater. Phys.*, 2007, **75**, 115127.
56 D. J. Gundlach, J. E. Royer, S. K. Park, S. Subramanian, O. D. Jurchescu, B. H. Hamadani, A. J. Moad, R. J. Kline, L. C. Teague, O. Kirillov, C. A. Richter, J. G. Kushmerick, L. J. Richter, S. R. Parkin, T. N. Jackson and J. E. Anthony, *Nat. Mater.*, 2008, **7**, 216–221.
57 M. R. Niazi, R. Li, M. Abdelsamie, K. Zhao, D. H. Anjum, M. M. Payne, J. Anthony, D.-M. Smilgies and A. Amassian, *Adv. Funct. Mater.*, 2016, **26**, 2371–2378.
58 S. K. Park, D. A. Mourey, S. Subramanian, J. E. Anthony and T. N. Jackson, *Appl. Phys. Lett.*, 2008, **93**, 043301.
59 S. G. J. Mathijssen, E. C. P. Smits, P. A. van Hal, H. J. Wondergem, S. A. Ponomarenko, A. Moser, R. Resel, P. A. Bobbert, M. Kemerink, R. A. J. Janssen and D. M. de Leeuw, *Nat. Nanotechnol.*, 2009, **4**, 674–680.
60 A. Carbone, B. K. Kotowska and D. Kotowski, *Phys. Rev. Lett.*, 2005, **95**, 236601.
61 D. V. Lang, X. Chi, T. Siegrist, A. M. Sergent and A. P. Ramirez, *Phys. Rev. Lett.*, 2004, **93**, 076601.
62 T.-Y. Chu and O.-K. Song, *Appl. Phys. Lett.*, 2007, **90**, 203512.
63 J. Lee, D. K. Hwang, C. H. Park, S. S. Kim and S. Im, *Thin Solid Films*, 2004, **451–452**, 12–15.
64 A. Carbone, C. Pennetta and L. Reggiani, *Appl. Phys. Lett.*, 2009, **95**, 233303.
65 O. Marinov and M. J. Deen, *2015 Int. Conf. Noise Fluctuations*, 2015, pp. 1–6.
66 M. J. Deen and O. Marinov, *20th Int. Conf. Noise Fluctuations*, 2009, pp. 197–200.
67 P. R. F. Rocha, H. L. Gomes, L. K. J. Vandamme, Q. Chen, A. Kiazadeh, D. M. de Leeuw and S. C. J. Meskers, *IEEE Trans. Electron Devices*, 2012, **59**, 2483–2487.
68 L. K. J. Vandamme, M. Cölle, D. M. de Leeuw and F. Verbakel, *Fluct. Noise Lett.*, 2011, **10**, 497–514.
69 B. F. Bory, P. R. F. Rocha, H. L. Gomes, D. M. de Leeuw and S. C. J. Meskers, *J. Appl. Phys.*, 2015, **118**, 205503.
70 Y. Song, H. Jeong, J. Jang, T.-Y. Kim, D. Yoo, Y. Kim, H. Jeong and T. Lee, *ACS Nano*, 2015, **9**, 7697–7703.
71 Y. Song, H. Jeong, S. Chung, G. H. Ahn, T.-Y. Kim, J. Jang, D. Yoo, H. Jeong, A. Javey and T. Lee, *Sci. Rep.*, 2016, **6**, 33967.
72 Y. Kim, H. Song, D. Kim, T. Lee and H. Jeong, *ACS Nano*, 2010, **4**, 4426–4430.
73 R. Arielly, M. Vadai, D. Kardash, G. Noy and Y. Selzer, *J. Am. Chem. Soc.*, 2014, **136**, 2674–2680.
74 D. Xiang, V. Sydoruk, S. Vitusevich, M. V. Petrychuk, A. Offenhäusser, V. A. Kochelap, A. E. Belyaev and D. Mayer, *Appl. Phys. Lett.*, 2015, **106**, 063701.
75 V. A. Sydoruk, D. Xiang, S. A. Vitusevich, M. V. Petrychuk, A. Vladyka, Y. Zhang, A. Offenhäusser, V. A. Kochelap, A. E. Belyaev and D. Mayer, *J. Appl. Phys.*, 2012, **112**, 014908.
76 M. Kiguchi, O. Tal, S. Wohlthat, F. Pauly, M. Krieger, D. Djukic, J. C. Cuevas and J. M. van Ruitenbeek, *Phys. Rev. Lett.*, 2008, **101**, 046801.
77 M. A. Karimi, S. G. Bahoosh, M. Herz, R. Hayakawa, F. Pauly and E. Scheer, *Nano Lett.*, 2016, **16**, 1803–1807.
78 Y. Kim, T. Pietsch, A. Erbe, W. Belzig and E. Scheer, *Nano Lett.*, 2011, **11**, 3734–3738.
79 S. Kogan, *Electronic Noise and Fluctuations in Solids*, Cambridge University Press, 2008.
80 Y. M. Blanter and M. Büttiker, *Phys. Rep.*, 2000, **336**, 1–166.
81 C. W. J. Beenakker and H. van Houten, *Phys. Rev. B: Condens. Matter Mater. Phys.*, 1991, **43**, 12066.
82 W. Schottky, *Ann. Phys.*, 1918, **362**, 541–567.
83 A. M. Cowley and R. A. Zettler, *IEEE Trans. Electron Devices*, 1968, **15**, 761–769.
84 A. Kumar, L. Saminadayar, D. C. Glattli, Y. Jin and B. Etienne, *Phys. Rev. Lett.*, 1996, **76**, 2778–2781.
85 M. Reznikov, M. Heiblum, H. Shtrikman and D. Mahalu, *Phys. Rev. Lett.*, 1995, **75**, 3340–3343.
86 R. S. Whitney and P. Jacquod, *Phys. Rev. Lett.*, 2006, **96**, 206804.
87 M. Henny, S. Oberholzer, C. Strunk, C. Schönenberger and C. Schonenberger, *Phys. Rev. B: Condens. Matter Mater. Phys.*, 1999, **59**, 2871–2880.
88 C. W. J. Beenakker and M. Büttiker, *Phys. Rev. B: Condens. Matter Mater. Phys.*, 1992, **46**, 1889–1892.
89 T. K. Djidjou, D. A. Bevans, S. Li and A. Rogachev, *IEEE Trans. Electron Devices*, 2014, **61**, 3252–3257.
90 K. K. Hung, P. K. Ko, C. Hu and Y. C. Cheng, *IEEE Electron Device Lett.*, 1990, **11**, 90–92.
91 M. J. Uren, D. J. Day and M. J. Kirton, *Appl. Phys. Lett.*, 1985, **47**, 1195–1197.
92 K. K. Hung, P.-K. Ko, C. Hu and Y. C. Cheng, *IEEE Trans. Electron Devices*, 1990, **37**, 654–665.
93 R. Soni, P. Meuffels, A. Petraru, M. Weides, C. Kügeler, R. Waser and H. Kohlstedt, *J. Appl. Phys.*, 2010, **107**, 024517.
94 S. Ambrogio, S. Balatti, A. Cubeta, A. Calderoni, N. Ramaswamy and D. Ielmini, *IEEE Trans. Electron Devices*, 2014, **61**, 2920–2927.
95 J.-K. Lee, H. Y. Jeong, I.-T. Cho, J. Y. Lee, S.-Y. Choi, H.-I. Kwon and J.-H. Lee, *IEEE Electron Device Lett.*, 2010, **31**, 603–605.
96 C. Dekker, A. Scholten, F. Liefrink, R. Eppenga, H. van Houten and C. T. Foxon, *Phys. Rev. Lett.*, 1991, **66**, 2148–2151.
97 D. Lachance-Quirion, S. Tremblay, S. A. Lamarre, V. Méthot, D. Gingras, J. Camirand Lemyre, M. Pioro-Ladrière and C. N. Allen, *Nano Lett.*, 2014, **14**, 882–887.
98 S. Kano, Y. Azuma, D. Tanaka, M. Sakamoto, T. Teranishi, L. W. Smith, C. G. Smith and Y. Majima, *J. Appl. Phys.*, 2013, **114**, 223717.
99 Y. Yuzhelevski, M. Yuzhelevski and G. Jung, *Rev. Sci. Instrum.*, 2000, **71**, 1681–1688.
100 C. M. Chang, S. S. Chung, Y. S. Hsieh, L. W. Cheng, C. T. Tsai, G. H. Ma, S. C. Chien and S. W. Sun, *IEDM Tech. Dig.*, 2008, 1–4.

101 Z. Çelik-Butler, P. Vasina and N. V. Amarasinghe, *IEEE Trans. Electron Devices*, 2000, **47**, 646–648.
102 F. M. Puglisi, P. Pavan, A. Padovani, L. Larcher and G. Bersuker, *Proc of IEEE ESSDERC*, 2012, 274–277.
103 S. Choi, Y. Yang and W. Lu, *Nanoscale*, 2014, **6**, 400–404.
104 M. Terai, Y. Sakotsubo, Y. Saito, S. Kotsuji and H. Hada, *IEEE Electron Device Lett.*, 2010, **31**, 1302–1304.
105 Y. Vardi, A. Guttman and I. Bar-Joseph, *Nano Lett.*, 2014, **14**, 2794–2799.
106 C. Surya and T. Y. Hsiang, *Phys. Rev. B: Condens. Matter Mater. Phys.*, 1986, **33**, 4898–4905.
107 C. T. Sah and F. H. Hielscher, *Phys. Rev. Lett.*, 1966, **17**, 956–958.
108 F. M. Klaassen, *IEEE Trans. Electron Devices*, 1971, **18**, 887–891.
109 M. Stoisiek and D. Wolf, *IEEE Trans. Electron Devices*, 1980, **27.9**, 1753–1757.
110 J. Rhayem, D. Rigaud, M. Valenza, N. Szydlo and H. Lebrun, *Solid-State Electron.*, 1999, **43**, 713–721.
111 J.-M. Lee, W.-S. Cheong, C.-S. Hwang, I.-T. Cho, H.-I. Kwon and J.-H. Lee, *IEEE Electron Device Lett.*, 2009, **30**, 505–507.
112 L. Ke, X. Y. Zhao, R. S. Kumar and S. J. Chua, *IEEE Electron Device Lett.*, 2006, **27**, 555–557.
113 S. Bychikhin, D. Pogany, L. K. J. Vandamme, G. Meneghesso and E. Zanoni, *J. Appl. Phys.*, 2005, **97**, 123714.
114 L. K. J. Vandamme, R. Alabedra and M. Zommiti, *Solid-State Electron.*, 1983, **26**, 671–674.
115 L. Jiang, E. R. Nowak, P. E. Scott, J. Johnson, J. M. Slaughter, J. J. Sun and R. W. Dave, *Phys. Rev. B: Condens. Matter Mater. Phys.*, 2004, **69**, 054407.
116 S.-H. Bae, J.-H. Lee, H.-I. Kwon, J.-R. Ahn, J.-C. Om, C. H. Park and J.-H. Lee, *IEEE Trans. Electron Devices*, 2009, **56**, 1624–1630.
117 N. Raghavan, D. D. Frey and K. L. Pey, *Microelectron. Reliab.*, 2014, **54**, 1729–1734.
118 Z. Fang, H. Y. Yu, J. A. Chroboczek, G. Ghibaudo, J. Buckley, B. De Salvo, X. Li and D. L. Kwong, *IEEE Trans. Electron Devices*, 2012, **59**, 850–853.
119 D. Lee, J. Lee, M. Jo, J. Park, M. Siddik and H. Hwang, *IEEE Electron Device Lett.*, 2011, **32**, 964–966.
120 F. N. Hooge, *IEEE Trans. Electron Devices*, 1994, **41**, 1926–1935.
121 F. N. Hooge, T. G. M. Kleinpenning and L. K. J. Vandamme, *Rep. Prog. Phys.*, 1981, **44**, 479–532.
122 F. N. Hooge, 1/f Noise Sources, *Advanced Experimental Methods for Noise Research in Nanoscale Electronic Devices*, Springer, Netherlands, 2004, pp. 3–10.
123 R. F. Voss, *J. Phys. C*, 1978, **11**, L923–L926.
124 R. F. Voss, *In 33rd Annu. Symp. Freq. Control.* 1979, pp. 40–46.
125 P. Dutta and P. M. Horn, *Rev. Mod. Phys.*, 1981, **53**, 497–516.
126 A. L. McWhorter, *1/f noise and related surface effects in germanium*, PhD dissertation, MIT, Cambridge, MA, 1955.
127 F. N. Hooge, *Phys. Lett. A*, 1969, **29**, 139–140.
128 F. N. Hooge, *Phys. B + C*, 1976, **83**, 14–23.
129 L. K. J. Vandamme, *In 2013 22nd Int. Conf. Noise Fluctuations, ICNF*, 2013, pp. 1–6.
130 G. Ghibaudo, O. Roux, C. Nguyen-Duc, F. Balestra and J. Brini, *Phys. Status Solidi*, 1991, **124**, 571–581.
131 P. Stallinga, *Electrical Characterization of Organic Electronic Materials and Devices*, John Wiley & Sons, 2009.
132 J. Gao, J. B. Xu, M. Zhu, N. Ke and D. Ma, *J. Phys. D: Appl. Phys.*, 2007, **40**, 5666–5669.
133 I. Kymissis, C. D. Dimitrakopoulos and S. Purushothaman, *IEEE Trans. Electron Devices*, 2001, **48**, 1060–1064.
134 L. G. Kaake, P. F. Barbara and X.-Y. Zhu, *J. Phys. Chem. Lett.*, 2010, **1**, 628–635.
135 B. Cho, S. Song, Y. Ji, T.-W. Kim and T. Lee, *Adv. Funct. Mater.*, 2011, **21**, 2806–2829.
136 Y. Song, J. Jang, D. Yoo, S.-H. Jung, S. Hong, J.-K. Lee and T. Lee, *Org. Electron.*, 2015, **17**, 192–197.
137 J. C. Scott and L. D. Bozano, *Adv. Mater.*, 2007, **19**, 1452–1463.
138 M. Cölle, M. Büchel and D. M. de Leeuw, *Org. Electron.*, 2006, **7**, 305–312.
139 H.-T. Lin, Z. Pei and Y.-J. Chan, *IEEE Electron Device Lett.*, 2007, **28**, 569–571.
140 S. B. Lee, S. Park, J. S. Lee, S. C. Chae, S. H. Chang, M. H. Jung, Y. Jo, B. Kahng, B. S. Kang, M.-J. Lee and T. W. Noh, *Appl. Phys. Lett.*, 2009, **95**, 122112.
141 D. Xiang, X. Wang, C. Jia, T. Lee and X. Guo, *Chem. Rev.*, 2016, **116**, 4318–4440.
142 G. Wang, T.-W. Kim and T. Lee, *J. Mater. Chem.*, 2011, **21**, 18117–18136.
143 N. J. Tao, *Nat. Nanotechnol.*, 2006, **1**, 173–181.
144 D. Djukic and J. M. van Ruitenbeek, *Nano Lett.*, 2006, **6**, 789–793.
145 R. J. Kline, M. D. McGehee, E. N. Kadnikova, J. Liu, J. M. J. Fréchet and M. F. Toney, *Macromolecules*, 2005, **38**, 3312–3319.
146 R. J. Kline, M. D. McGehee, E. N. Kadnikova, J. Liu and J. M. J. Fréchet, *Adv. Mater.*, 2003, **15**, 1519–1522.
147 P. Peumans, A. Yakimov and S. R. Forrest, *J. Appl. Phys.*, 2002, **93**, 3693–3723.
148 F. Guo, B. Yang, Y. Yuan, Z. Xiao, Q. Dong, Y. Bi and J. Huang, *Nat. Nanotechnol.*, 2012, **7**, 798–802.
149 Y. Fang, F. Guo, Z. Xiao and J. Huang, *Adv. Opt. Mater.*, 2014, **2**, 348–353.
150 S. Xiong, L. Li, F. Qin, L. Mao, B. Luo, Y. Jiang, Z. Li, J. Huang and Y. Zhou, *ACS Appl. Mater. Interfaces*, 2017, **9**, 9176–9183.
151 Y. Kim, T. J. Hellmuth, D. Sysoiev, F. Pauly, T. Pietsch, J. Wolf, A. Erbe, T. Huhn, U. Groth, U. E. Steiner and E. Scheer, *Nano Lett.*, 2012, **12**, 3736–3742.
152 H. Song, Y. Kim, Y. H. Jang, H. Jeong, M. A. Reed and T. Lee, *Nature*, 2009, **462**, 1039–1043.